

ENTROPY STABLE p -NONCONFORMING DISCRETIZATIONS WITH THE SUMMATION-BY-PARTS PROPERTY FOR THE COMPRESSIBLE EULER EQUATIONS *

DAVID C. DEL REY FERNÁNDEZ[†], MARK H. CARPENTER[‡], LISANDRO DALCIN[§],
LUCAS FREDRICH[¶], DIEGO ROJAS[§], ANDREW R. WINTERS^{||}, GREGOR J. GASSNER[¶]
, STEFANO ZAMPINI[§], AND MATTEO PARSANI[§]

Abstract. The entropy conservative/stable algorithm of Friedrich *et al.* (2018) for hyperbolic conservation laws on nonconforming p -refined/coarsened Cartesian grids, is extended to curvilinear grids for the compressible Euler equations. The primary focus is on constructing appropriate coupling procedures across the curvilinear nonconforming interfaces. A simple and flexible approach is proposed that uses interpolation operators from one element to the other. On the element faces, the analytic metrics are used to construct coupling terms, while metric terms in the volume are approximated to satisfy a discretization of the geometric conservation laws. The resulting scheme is entropy conservative/stable, elementwise conservative, and freestream preserving. The accuracy and stability properties of the resulting numerical algorithm are shown to be comparable to those of the original conforming scheme ($\sim p + 1$ convergence) in the context of the isentropic Euler vortex and the inviscid Taylor–Green vortex problems on manufactured high order grids.

Key words. nonconforming interfaces, nonlinear entropy stability, summation-by-parts operators, simultaneous-approximation-terms, high-order accurate discretizations, curved elements, unstructured grid

AMS subject classifications.

1 Introduction High-order accurate finite element methods (FEM) provide an efficient approach to achieve high solution accuracy. Their computational kernels are arithmetically dense making them compatible with the current and future highly concurrent hardware. In addition, they are amenable to h -, p -, and r -refinement algorithms, thus facilitating the redistribution of the degrees of freedom to better resolve multiscale physics.

High-order accurate methods are known to be more efficient than low-order methods for linear wave propagation [29, 45]. Although high order discretizations have a long history of development, their application to nonlinear partial differential equations (PDEs) for practical applications has been limited by robustness issues. Thus, nominally second-order accurate discretization operators are typically used in commercial and industrial software.

The summation-by-parts (SBP) framework provides a systematic and discretization-agnostic methodology for constructing arbitrarily high-order accurate and provably stable numerical methods for linear and variable coefficient linear problems (see, for

*Associated with this paper is a companion NASA technical report [15] that contains additional details omitted in this paper for brevity.

[†]National Institute of Aerospace and Computational AeroSciences Branch, NASA Langley Research Center, Hampton, VA, United States, (dcdelrey@gmail.com).

[‡]Computational AeroSciences Branch, NASA Langley Research Center, Hampton, VA, United States, (mark.h.carpenter@nasa.gov).

[§]King Abdullah University of Science and Technology (KAUST), Computer Electrical and Mathematical Science and Engineering Division (CEMSE), Extreme Computing Research Center (ECRC), Thuwal, Saudi Arabia, (dalcinl@gmail.com, diego.rojasblanco@kaust.edu.sa, stefano.zampini@kaust.edu.sa, matteo.parsani@kaust.edu.sa).

[¶]Mathematical Institute, University of Cologne, North Rhine-Westphalia, Germany, (lfriedri@math.uni-koeln.de, ggassner@math.uni-koeln.de).

^{||}Department of Mathematics (MAI), Linköping University, Sweden, (andrew.ross.winters@liu.se).

instance, the survey papers [17, 44]). SBP operators can be viewed as matrix difference operators that are mimetic of integration by parts in that they have a telescoping property. Discrete stability over the whole domain is achieved by combining the SBP mechanics with suitable inter-element coupling procedures and boundary conditions (e.g., the simultaneous approximation terms (SATs) [5, 31]).

For nonlinear problems, progress towards provably stable algorithms applicable to practical problems has been much slower. However, certain class of nonlinear conservation laws come endowed with a complementary inequality statement (equality for smooth solutions) on the mathematical entropy (see, for instance, [12]). Therefore, it is desirable for the numerical method to satisfy a corresponding discrete analogue. This can then be used to prove nonlinear stability of the numerical scheme [46, 47]. Along these lines, a productive trajectory was initiated by Tadmor [46] who constructed entropy conservative low-order finite volume schemes that achieve entropy conservation by using two-point flux functions that when contracted with the entropy variables result in a telescoping entropy flux. Entropy stability was ensured by adding appropriate dissipation. Through the telescoping property, the continuous L^2 entropy stability analysis is mimicked by the semi-discrete stability analysis (for a review of these ideas see Tadmor [47]). Tadmor's basic idea has led to the construction of a number of high order and low order entropy stable schemes (see, for instance, [22, 37]). An alternative approach, developed by Olsson and Oliger [32], Gerritsen and Olsson [25] and Yee *et al.* [53] (see also [38, 39]), relies on choosing entropy functions that result in a homogeneity property on the Euler fluxes. By using this property, splittings of the Euler fluxes are constructed such that when contracted with the entropy variables result in stability estimates analogous in form to energy estimates obtained for linear PDEs. Thus, discretizing the resulting split form using SBP operators, the nonlinear stability analysis performed at the continuous level is mimicked at the semi-discrete level.

A complementary extension of Tadmor's ideas to finite domains was initiated by Fisher and coworkers who combined the SBP framework, using classical finite difference SBP operators, with Tadmor's two-point flux [19, 21, 20]. The resulting schemes follow the continuous entropy analysis and can be shown to be entropy conservative and be made entropy stable by adding appropriate interface dissipation. This nonlinearly stable approach inherits all the mechanics of linear SBP schemes for the imposition of boundary conditions and inter-element coupling and therefore gives a systematic methodology for discretizing problems on complex geometries [3, 34, 35]. Moreover, by constructing schemes that are discretely mimetic of the continuous stability analysis, the need to assume exact integration in the stability proofs is eliminated (see for example the work of Hughes *et al.* [26]). These ideas have been extended to include collocated spectral elements [3], fully- and semi-staggered spectral elements [33, 7], Cartesian, semi-staggered, nonconforming p -refinement [7], WENO spectral collocation [52], multidimensional SBP operators [11, 10], multidimensional staggered SBP operators [16], modal decoupled SBP operators [8], and fully discrete explicit entropy stable schemes [23, 36], as well as to a number of PDEs besides the compressible Euler and Navier–Stokes equations (for example the magnetohydrodynamics [50] and the shallow water [51] equations).

A necessary constraint for entropy stability on curvilinear meshes is satisfaction of discrete geometric conservation law (GCL) conditions [19, 21, 3, 33]. Well documented procedures exist for generating discrete transformation metrics on conforming meshes that satisfy the GCL conditions [48, 49]. These procedures extend immediately to the nonconforming case provided that the polynomial order of the method is sufficient

to analytically resolve the element surface transformation metrics; a condition that is naturally satisfied if the polynomial orders of the geometry, p_g and discretization, p , are related by the inequality $p_g \leq \frac{p+1}{2}$. While it is possible to generate body fitted meshes with full geometric surface order ($p_g = p$) and reduced off body order $p_g \leq \frac{p+1}{2}$, this forces undue complexity on the already complex task of grid generation. Enforcing the $p_g = p$ grid constraint on near-body elements, while avoiding grid line cross-over or negative Jacobians, increases in complexity with mesh aspect ratio, and is virtually impossible to achieve in the high Reynolds number limit of realistic aerodynamic configurations.

Herein, the primary objective is to construct entropy stable discretizations suitable for the mechanics of high order FEM p -adaptivity, applicable for general meshes containing hexahedral polynomial elements of full geometric order (i.e., $p_g \leq p$). Initial nonconforming efforts focused on Cartesian, semi-staggered spectral collocation operators [7], but identifying a curvilinear extension has proven difficult. Thus, this work extends to curvilinear coordinates the Cartesian grid work previously reported by Friedrich *et al.* [24], and primarily focuses on constructing appropriate coupling procedures across curvilinear nonconforming interfaces.

Many novel contributions are included in this work. They are summarized as follows:

- A general, yet simple entropy stable nonconforming algorithm is proposed in curvilinear coordinates for the compressible Euler equations that
 - Encapsulates and generalizes several approaches for coupling curvilinear nonconforming interfaces
 - Formalizes necessary conditions for entropy conservation at curvilinear nonconforming interfaces
 - Elegantly handles various mesh generation strategies including elements of full geometric order ($p_g \leq p$)
 - Extends the metric approximation approach of Crean *et al.* [11] to curvilinear nonconforming interfaces
 - Satisfies the discrete GCL conditions, therefore ensuring freestream preservation
 - Exploits the generality of distinct surface and volume metrics that couple through the GCL constraint
- Numerical evidence is provided that supports the assertion that the conforming [3, 33] and nonconforming algorithms exhibit similar 1) nonlinear robustness properties and 2) L^2 -norm convergence rates, (i.e., nominally $p + 1$ for polynomials of degree p).

The paper is organized as follows: Section 2 delineates the notation used herein. The nonconforming algorithm is presented in the simple context of the convection equation in Section 3. This is followed by an introduction to the construction of nonlinearly stable schemes by examining the discretization of the Burgers' equation (Section 4). The nonconforming algorithm presented in Section 3 and the mechanics presented in Section 4 are combined in Section 5 to construct an entropy conservative/stable nonconforming discretization for the compressible Euler equations. Numerical experiments are given in Section (7), while conclusions are drawn in Section 8.

2 Notation PDEs are discretized on cubes having Cartesian computational coordinates denoted by the triple (ξ_1, ξ_2, ξ_3) , where the physical coordinates are denoted by the triple (x_1, x_2, x_3) . Vectors are represented by lowercase bold font, for example

\mathbf{u} , while matrices are represented using sans-serif font, for example, \mathbf{B} . Continuous functions on a space-time domain are denoted by capital letters in script font. For example,

$$\mathcal{U}(\xi_1, \xi_2, \xi_3, t) \in L^2([\alpha_1, \beta_1] \times [\alpha_2, \beta_2] \times [\alpha_3, \beta_3] \times [0, T])$$

represents a square integrable function, where t is the temporal coordinate. The restriction of such functions onto a set of mesh nodes is denoted by lower case bold font. For example, the restriction of \mathcal{U} onto a grid of $N_1 \times N_2 \times N_3$ nodes is given by the vector

$$\mathbf{u} = \left[\mathcal{U}(\boldsymbol{\xi}^{(1)}, t), \dots, \mathcal{U}(\boldsymbol{\xi}^{(N)}, t) \right]^T,$$

where, N is the total number of nodes ($N \equiv N_1 N_2 N_3$) square brackets ($[]$) are used to delineate vectors and matrices as well as ranges for variables (the context will make clear which meaning is being used). Moreover, $\boldsymbol{\xi}$ is a vector of vectors constructed from the three vectors $\boldsymbol{\xi}_1$, $\boldsymbol{\xi}_2$, and $\boldsymbol{\xi}_3$, which are vectors of size N_1 , N_2 , and N_3 and contain the coordinates of the mesh in the three computational directions, respectively. Finally, $\boldsymbol{\xi}$ is constructed as

$$\boldsymbol{\xi}(3(i-1) + 1 : 3i) \equiv \boldsymbol{\xi}^{(i)} \equiv [\boldsymbol{\xi}_1(i), \boldsymbol{\xi}_2(i), \boldsymbol{\xi}_3(i)]^T,$$

where the notation $\mathbf{u}(i)$ means the i^{th} entry of the vector \mathbf{u} and $\mathbf{u}(i : j)$ is the subvector constructed from \mathbf{u} using the i^{th} through j^{th} entries (i.e., Matlab notation is used).

Oftentimes, monomials are discussed and the following notation is used:

$$\boldsymbol{\xi}_l^j \equiv \left[(\xi_l(1))^j, \dots, (\xi_l(N_l))^j \right]^T,$$

and the convention that $\boldsymbol{\xi}_l^j = \mathbf{0}$ for $j < 0$ is used.

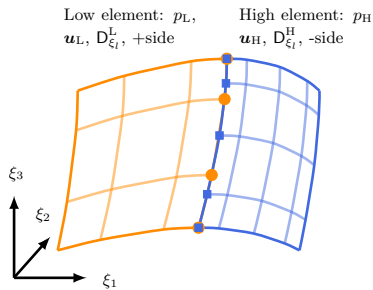
Herein, one-dimensional SBP operators are used to discretize derivatives. The definition of a one-dimensional SBP operator in the ξ_l direction, $l = 1, 2, 3$, is [14, 17, 44]

DEFINITION 2.1. *Summation-by-parts operator for the first derivative:* A matrix operator with constant coefficients, $\mathbf{D}_{\xi_l}^{(1D)} \in \mathbb{R}^{N_l \times N_l}$, is a linear SBP operator of degree p approximating the derivative $\frac{\partial}{\partial \xi_l}$ on the domain $\xi_l \in [\alpha_l, \beta_l]$ with nodal distribution $\boldsymbol{\xi}_l$ having N_l nodes, if

1. $\mathbf{D}_{\xi_l}^{(1D)} \boldsymbol{\xi}_l^j = j \boldsymbol{\xi}_l^{j-1}$, $j = 0, 1, \dots, p$;
2. $\mathbf{D}_{\xi_l}^{(1D)} \equiv \left(\mathbf{P}_{\xi_l}^{(1D)} \right)^{-1} \mathbf{Q}_{\xi_l}^{(1D)}$, where the norm matrix, $\mathbf{P}_{\xi_l}^{(1D)}$, is symmetric positive definite;
3. $\mathbf{Q}_{\xi_l}^{(1D)} \equiv \left(\mathbf{S}_{\xi_l}^{(1D)} + \frac{1}{2} \mathbf{E}_{\xi_l}^{(1D)} \right)$, $\mathbf{S}_{\xi_l}^{(1D)} = - \left(\mathbf{S}_{\xi_l}^{(1D)} \right)^T$, $\mathbf{E}_{\xi_l}^{(1D)} = \left(\mathbf{E}_{\xi_l}^{(1D)} \right)^T$, $\mathbf{E}_{\xi_l}^{(1D)} = \text{diag}(-1, 0, \dots, 0, 1) = \mathbf{e}_{N_l} \mathbf{e}_{N_l}^T - \mathbf{e}_1 \mathbf{e}_1^T$, $\mathbf{e}_1 \equiv [1, 0, \dots, 0]^T$, and $\mathbf{e}_{N_l} \equiv [0, 0, \dots, 1]^T$.

Thus, a degree p SBP operator is one that differentiates exactly monomials up to degree p .

In this work, one-dimensional SBP operators are extended to multiple dimensions using tensor products (\otimes). The tensor product between the matrices \mathbf{A} and \mathbf{B} is given as $\mathbf{A} \otimes \mathbf{B}$. When referencing individual entries in a matrix the notation $\mathbf{A}(i, j)$ is used, which means the i^{th} j^{th} entry in the matrix \mathbf{A} . The Hadamard product (\circ) is also used in the construction of entropy conservative/stable discretizations. For example,

FIG. 1. *Nonconforming elements.*

the Hadamard product between the matrices \mathbf{A} and \mathbf{B} is given by $\mathbf{A} \circ \mathbf{B}$.

The focus in this paper is exclusively on diagonal-norm SBP operators. Moreover, the same one-dimensional SBP operator are used in each direction, each operating on N nodes. Specifically, diagonal-norm SBP operators constructed on the Legendre–Gauss–Lobatto (LGL) nodes are used, i.e., a discontinuous Galerkin collocated spectral element approach is utilized.

The physical domain $\Omega \subset \mathbb{R}^3$, with boundary $\Gamma \equiv \partial\Omega$ is partitioned into K non-overlapping hexahedral elements. The domain of the κ^{th} element is denoted by Ω_κ and has boundary $\partial\Omega_\kappa$. Numerically, PDEs are solved in computational coordinates, where each Ω_κ is locally transformed to $\hat{\Omega}_\kappa$, with boundary $\hat{\Gamma} \equiv \partial\hat{\Omega}_\kappa$, under the following assumption:

ASSUMPTION 1. *Each element in physical space is transformed using a local and invertible curvilinear coordinate transformation that is compatible at shared interfaces, meaning that points in computational space on either side of a shared interface mapped to the same physical location and therefore map back to the analogous location in computational space; this is the standard assumption that the curvilinear coordinate transformation is water tight.*

3 A p -nonconforming algorithm: Linear convection The focus herein is on nonconformity arising from curvilinearly mapped elements that have conforming interfaces but nonconforming nodal distributions, as would result from p -refinement interfaces (see Fig. 1). The construction of entropy conservative/stable discretizations for the compressible Euler equations on Cartesian grids is detailed in Friedrich *et al.* [24]. Extending the Cartesian work involves developing a p -refinement, curvilinear, interface coupling technique that maintains 1) accuracy, 2) discrete entropy conservation/stability, and 3) elementwise conservation.

3.1 Scalar convection: continuous and semi-discrete analysis Many of the salient difficulties encountered while constructing stable and conservative nonconforming discretizations of the Euler equations, are also present in discretization of linear convection. Consider the constant coefficient linear convection in Cartesian coordinates.

$$(3.1) \quad \frac{\partial \mathcal{U}}{\partial t} + \sum_{m=1}^3 \frac{\partial (a_m \mathcal{U})}{\partial x_m} = 0,$$

where $(a_m \mathcal{U})$ are the fluxes and a_m are the (constant) components of the convection speed. The stability of (3.1) can be determined using the energy method which proceeds by multiplying (3.1) by the solution (\mathcal{U}) , and after using the chain rule

results in

$$(3.2) \quad \frac{1}{2} \frac{\partial \mathcal{U}^2}{\partial t} + \frac{1}{2} \sum_{m=1}^3 \frac{\partial (a_m \mathcal{U}^2)}{\partial x_m} = 0.$$

Integrating over the domain, Ω , using integration by parts, and Leibniz rule gives

$$(3.3) \quad \frac{d}{dt} \int_{\Omega} \frac{\mathcal{U}^2}{2} d\Omega + \frac{1}{2} \sum_{m=1}^3 \oint_{\Gamma} (a_m \mathcal{U}^2) n_{x_m} d\Gamma = 0,$$

where n_{x_m} is the m^{th} component of the outward facing unit normal. What Eq. (3.3) demonstrates is that the time rate of change of the norm of the solution, $\|\mathcal{U}\|^2 \equiv \int_{\Omega} \mathcal{U}^2 d\Omega$, depends solely on surface flux integrals. Imposing appropriate boundary conditions in Eq. (3.3) leads to an energy estimate on the solution and therefore a proof of stability. The discretizations that are developed in this paper mimic the above energy analysis in a one-to-one fashion and similarly lead to stability statements on the semi-discrete equations.

The proposed algorithm is constructed from differentiation matrices that live in computational space and for this purpose, Eq. (3.1) is transformed using the curvilinear coordinate transformation $x_m = x_m(\xi_1, \xi_2, \xi_3)$. Thus, after expanding the derivatives as

$$\frac{\partial}{\partial x_m} = \sum_{l=1}^3 \frac{\partial \xi_l}{\partial x_m} \frac{\partial}{\partial \xi_l},$$

and multiplying by the metric Jacobian (\mathcal{J}_{κ}), (3.1) becomes

$$(3.4) \quad \mathcal{J}_{\kappa} \frac{\partial \mathcal{U}}{\partial t} + \sum_{l,m=1}^3 \mathcal{J}_{\kappa} \frac{\partial \xi_l}{\partial x_m} \frac{\partial (a_m \mathcal{U})}{\partial \xi_l} = 0.$$

Herein, we refer to Eq. (3.4) as the chain rule form of Eq. (3.1). Bringing the metric terms, $\mathcal{J}_{\kappa} \frac{\partial \xi_l}{\partial x_m}$, inside the derivative and using the product rule gives

$$(3.5) \quad \mathcal{J}_{\kappa} \frac{\partial \mathcal{U}}{\partial t} + \sum_{l,m=1}^3 \frac{\partial}{\partial \xi_l} \left(\mathcal{J}_{\kappa} \frac{\partial \xi_l}{\partial x_m} a_m \mathcal{U} \right) - \sum_{l,m=1}^3 a_m \mathcal{U} \frac{\partial}{\partial \xi_l} \left(\mathcal{J}_{\kappa} \frac{\partial \xi_l}{\partial x_m} \right) = 0.$$

The last term on the left-hand side of (3.5) is zero via the GCL relations

$$(3.6) \quad \sum_{l=1}^3 \frac{\partial}{\partial \xi_l} \left(\mathcal{J}_{\kappa} \frac{\partial \xi_l}{\partial x_m} \right) = 0, \quad m = 1, 2, 3,$$

leading to the strong conservation form of the convection equation in curvilinear coordinates:

$$(3.7) \quad \mathcal{J}_{\kappa} \frac{\partial \mathcal{U}}{\partial t} + \sum_{l,m=1}^3 \frac{\partial}{\partial \xi_l} \left(\mathcal{J}_{\kappa} \frac{\partial \xi_l}{\partial x_m} a_m \mathcal{U} \right) = 0.$$

Now, consider discretizing (3.7) by using the following differentiation matrices:

$$\mathbf{D}_{\xi_1} \equiv \mathbf{D}^{(1D)} \otimes \mathbf{I}_N \otimes \mathbf{I}_N, \quad \mathbf{D}_{\xi_2} \equiv \mathbf{I}_N \otimes \mathbf{D}^{(1D)} \otimes \mathbf{I}_N, \quad \mathbf{D}_{\xi_3} \equiv \mathbf{I}_N \otimes \mathbf{I}_N \otimes \mathbf{D}^{(N)},$$

where \mathbf{I}_N is an $N \times N$ identity matrix. The diagonal matrices containing the metric

Jacobian and metric terms along their diagonals, respectively, are defined as follows:

$$\begin{aligned} \mathbf{J}_\kappa &\equiv \text{diag} \left(\mathcal{J}_\kappa(\boldsymbol{\xi}^{(1)}), \dots, \mathcal{J}_\kappa(\boldsymbol{\xi}^{(N_\kappa)}) \right), \\ \left[\mathcal{J} \frac{\partial \xi_l}{\partial x_m} \right]_\kappa &\equiv \text{diag} \left(\mathcal{J}_\kappa \frac{\partial \xi_l}{\partial x_m}(\boldsymbol{\xi}^{(1)}), \dots, \mathcal{J}_\kappa \frac{\partial \xi_l}{\partial x_m}(\boldsymbol{\xi}^{(N_\kappa)}) \right). \end{aligned}$$

where $N_\kappa \equiv N^3$ is the total number of nodes in element κ . With this nomenclature, the discretization of (3.7) on the κ^{th} element reads

$$(3.8) \quad \mathbf{J}_\kappa \frac{d\mathbf{u}_\kappa}{dt} + \sum_{l,m=1}^3 \mathbf{D}_{\xi_l} \left[\mathcal{J} \frac{\partial \xi_l}{\partial x_m} \right]_\kappa a_m \mathbf{u}_\kappa = \mathbf{SAT},$$

where \mathbf{SAT} is the vector of the SATs used to impose both boundary conditions and or inter-element connectivity. Unfortunately, the scheme (3.8) is not guaranteed to be stable. However, a well-known remedy is to consider a canonical splitting which is arrived at by summing one half of (3.4) and one half of (3.5), giving

$$(3.9) \quad \begin{aligned} &\mathcal{J}_\kappa \frac{\partial \mathcal{U}}{\partial t} + \frac{1}{2} \sum_{l,m=1}^3 \left\{ \frac{\partial}{\partial \xi_l} \left(\mathcal{J}_\kappa \frac{\partial \xi_l}{\partial x_m} a_m \mathcal{U} \right) + \mathcal{J}_\kappa \frac{\partial \xi_l}{\partial x_m} \frac{\partial}{\partial \xi_l} (a_m \mathcal{U}) \right\} \\ &- \frac{1}{2} \sum_{l,m=1}^3 \left\{ a_m \mathcal{U} \frac{\partial}{\partial \xi_l} \left(\mathcal{J}_\kappa \frac{\partial \xi_l}{\partial x_m} \right) \right\} = 0, \end{aligned}$$

where the last set of terms are zero by the GCL conditions (3.6). Then, a stable semi-discrete form is constructed in the same manner as the split form (3.9) by discretizing (3.4) and (3.5) using \mathbf{D}_{ξ_l} , \mathbf{J}_κ , and $\left[\mathcal{J} \frac{\partial \xi_l}{\partial x_m} \right]_\kappa$, and averaging the results. This procedure yields

$$(3.10) \quad \begin{aligned} &\mathbf{J}_\kappa \frac{d\mathbf{u}_\kappa}{dt} + \frac{1}{2} \sum_{l,m=1}^3 a_m \left\{ \mathbf{D}_{\xi_l} \left[\mathcal{J} \frac{\partial \xi_l}{\partial x_m} \right]_\kappa + \left[\mathcal{J} \frac{\partial \xi_l}{\partial x_m} \right]_\kappa \mathbf{D}_{\xi_l} \right\} \mathbf{u}_\kappa \\ &- \frac{1}{2} \sum_{l,m=1}^3 \left\{ a_m \text{diag}(\mathbf{u}_\kappa) \mathbf{D}_{\xi_l} \left[\mathcal{J} \frac{\partial \xi_l}{\partial x_m} \right]_\kappa \mathbf{1}_\kappa \right\} = \mathbf{0}, \end{aligned}$$

where $\mathbf{1}_\kappa$ is a vector of ones of the size of the number of nodes on the κ^{th} element. As in the continuous case, the semi-discrete form has a set of discrete GCL conditions

$$(3.11) \quad \sum_{l=1}^3 \mathbf{D}_{\xi_l} \left[\mathcal{J} \frac{\partial \xi_l}{\partial x_m} \right]_\kappa \mathbf{1}_\kappa = \mathbf{0}, \quad m = 1, 2, 3,$$

that if satisfied, lead to the following telescoping (provably stable) semi-discrete form

$$(3.12) \quad \mathbf{J}_\kappa \frac{d\mathbf{u}_\kappa}{dt} + \frac{1}{2} \sum_{l,m=1}^3 a_m \left\{ \mathbf{D}_{\xi_l} \left[\mathcal{J} \frac{\partial \xi_l}{\partial x_m} \right]_\kappa + \left[\mathcal{J} \frac{\partial \xi_l}{\partial x_m} \right]_\kappa \mathbf{D}_{\xi_l} \right\} \mathbf{u}_\kappa = \mathbf{0}.$$

Remark 3.1. The linear stability of semi-discrete operators for constant coefficient hyperbolic systems, is not preserved by arbitrary design order approximations to the metric terms. Only approximations to the metric terms that satisfy discrete GCL (3.11) conditions lead to stable semi-discrete forms, a point that can not be overemphasized in the context of this work.

Remark 3.2. The satisfaction of the discrete GCL conditions (3.11) for tensor-product conforming discretizations has well-known solutions (Vinokur and Yee [49] or Thomas and Lombard [48]) which require that the differentiation matrices commute,

i.e. $D_{\xi_1} D_{\xi_2} = D_{\xi_2} D_{\xi_1}$, etc..

Remark 3.3. The discrete GCL conditions can alternatively be derived by inputting a constant solution into (3.10).

3.2 Scalar convection and the nonconforming interface The analysis and presentation of nonconforming semi-discrete algorithms is simplified by considering a single interface between two adjoining elements as shown in Figure 1. The elements have aligned computational coordinates and the shared interface is vertical. The nonconformity is assumed to arise from local approximations with differing polynomial degrees. Specifically, the left element has polynomial degree p_L (low: subscript/superscript L) and the right element has polynomial degree p_H (high: subscript/superscript H) where $p_H > p_L$ (see Figure 1). The first task is to construct SBP operators that span both elements: i.e., macro element operators composed of elements L and H. A naive construction would be the following operators in the three coordinate directions:

$$(3.13) \quad \tilde{D}_{\xi_1} \equiv \begin{bmatrix} D_{\xi_1}^L & \\ & D_{\xi_1}^H \end{bmatrix} \quad ; \quad \tilde{D}_{\xi_2} \equiv \begin{bmatrix} D_{\xi_2}^L & \\ & D_{\xi_2}^H \end{bmatrix} \quad ; \quad \tilde{D}_{\xi_3} \equiv \begin{bmatrix} D_{\xi_3}^L & \\ & D_{\xi_3}^H \end{bmatrix}$$

The \tilde{D}_{ξ_2} and \tilde{D}_{ξ_3} macro element operators are by construction SBP operators; the action of their differentiation is parallel to the interface, and they telescope out to the boundaries. The \tilde{D}_{ξ_1} is not by construction an SBP operator, despite the individual matrices composing \tilde{D}_{ξ_1} being SBP operators. In addition, and more critically, there is no coupling between the two elements. Thus, interface coupling must be introduced between the two elements that render the operators on the macro element as SBP operators. For this purpose, interpolation operators are needed that interpolate information from element H to element L and vice versa. For simplicity, the interpolation operators use only tensor product surface information from the adjoining interface surface.

With this background, general matrix difference operators between the two elements are constructed as

$$(3.14) \quad \tilde{D}_{\xi_l} = \tilde{P}^{-1} \tilde{Q}_{\xi_l} = \tilde{P}^{-1} \left(\tilde{S}_{\xi_l} + \frac{1}{2} \tilde{E}_{\xi_l} \right).$$

Focusing on the direction orthogonal to the interface (ξ_1) the relevant matrices are given by

$$(3.15) \quad \tilde{P} \equiv \text{diag} \begin{bmatrix} P^L & \\ & P^H \end{bmatrix},$$

$$\tilde{S}_{\xi_1} \equiv \begin{bmatrix} S_{\xi_1}^L & \frac{1}{2} \left(e_{N_L} e_{1_H}^T \otimes P_L^{(1D)} I_{HtoL}^{(1D)} \otimes P_L^{(1D)} I_{HtoL}^{(1D)} \right) \\ -\frac{1}{2} \left(e_{1_H} e_{N_L}^T \otimes P_H^{(1D)} I_{LtoH}^{(1D)} \otimes P_H^{(1D)} I_{LtoH}^{(1D)} \right) & S_{\xi_1}^H \end{bmatrix},$$

$$\tilde{E}_{\xi_1} \equiv \begin{bmatrix} -e_{1_L} e_{1_L}^T \otimes P_L^{(1D)} \otimes P_L^{(1D)} & \\ & e_{N_H} e_{N_H}^T \otimes P_H^{(1D)} \otimes P_H^{(1D)} \end{bmatrix},$$

and $I_{HtoL}^{(1D)}$ and $I_{LtoH}^{(1D)}$ are one-dimensional interpolation operators from the H element to the L element and vice versa.

A necessary constraint the SBP formalism places on \tilde{D}_{ξ_1} , is skew-symmetry of the

$\tilde{\mathcal{S}}_{\xi_1}$ matrices. The block-diagonal matrices in $\tilde{\mathcal{S}}_{\xi_1}$ are already skew-symmetric but the off diagonal blocks are not. Thus, it is necessary to satisfy the following condition:

$$\left(\mathbf{e}_{N_L} \mathbf{e}_{1_H}^T \otimes \mathbf{P}_L^{(1D)} \mathbf{l}_{\text{HtoL}}^{(1D)} \otimes \mathbf{P}_L^{(1D)} \mathbf{l}_{\text{HtoL}}^{(1D)} \right) = \left\{ \left(\mathbf{e}_{1_H} \mathbf{e}_{N_L}^T \otimes \mathbf{P}_H^{(1D)} \mathbf{l}_{\text{LtoH}}^{(1D)} \otimes \mathbf{P}_H^{(1D)} \mathbf{l}_{\text{LtoH}}^{(1D)} \right) \right\}^T.$$

This implies that the interpolation operators are related to each other as follows:

$$\mathbf{l}_{\text{HtoL}}^{(1D)} = \left(\mathbf{P}_L^{(1D)} \right)^{-1} \left(\mathbf{l}_{\text{LtoH}}^{(1D)} \right)^T \mathbf{P}_H^{(1D)}.$$

This property is denoted as the SBP preserving property because it leads to a macro element differentiation matrix that is an SBP operator. The optimal interpolation operator, $\mathbf{l}_{\text{LtoH}}^{(1D)}$, is constructed to exactly interpolate polynomial of degree p_L and can be easily constructed as follows:

$$\mathbf{l}_{\text{LtoH}}^{(1D)} = [\boldsymbol{\xi}_H^0, \dots, \boldsymbol{\xi}_H^{p_L}] [\boldsymbol{\xi}_L^0, \dots, \boldsymbol{\xi}_L^{p_L}]^{-1},$$

where $\boldsymbol{\xi}_L$ and $\boldsymbol{\xi}_H$ are the one-dimensional nodal distributions in computational space of the two elements. The companion interpolation operator $\mathbf{l}_{\text{HtoL}}^{(1D)}$ is sub-optimal by one degree ($p_L - 1$), a consequence of satisfying the necessary SBP-preserving property (see Friedrich *et al.* [24] for a complete discussion).

The semi-discrete skew-symmetric split operator given in Eq. (3.10), discretized using the macro element operators $\tilde{\mathbf{D}}_{\xi_l}$, and metric information \mathbf{J} , $\left[\mathcal{J} \frac{\partial \xi_l}{\partial x_m} \right]$, leads to the following:

$$(3.16) \quad \begin{aligned} \mathbf{J} \frac{d\tilde{\mathbf{u}}}{dt} + \frac{1}{2} \sum_{l,m=1}^3 a_m \left(\tilde{\mathbf{D}}_{\xi_l} \left[\mathcal{J} \frac{\partial \xi_l}{\partial x_m} \right] + \left[\mathcal{J} \frac{\partial \xi_l}{\partial x_m} \right] \tilde{\mathbf{D}}_{\xi_l} \right) \tilde{\mathbf{u}} \\ - \frac{1}{2} \sum_{l,m=1}^3 a_m \text{diag}(\tilde{\mathbf{u}}) \tilde{\mathbf{D}}_{\xi_l} \left[\mathcal{J} \frac{\partial \xi_l}{\partial x_m} \right] \tilde{\mathbf{i}} = \mathbf{0}, \end{aligned}$$

where

$$(3.17) \quad \tilde{\mathbf{u}} \equiv [\mathbf{u}_L^T, \mathbf{u}_H^T]^T, \mathbf{J} \equiv \text{diag} \begin{bmatrix} \mathbf{J}_L & & \\ & \mathbf{J}_H & \\ & & \end{bmatrix}, \left[\mathcal{J} \frac{\partial \xi_l}{\partial x_m} \right] \equiv \begin{bmatrix} \left[\mathcal{J} \frac{\partial \xi_l}{\partial x_m} \right]_L & & \\ & & \left[\mathcal{J} \frac{\partial \xi_l}{\partial x_m} \right]_H \end{bmatrix}.$$

As was the case in Eq. (3.10), a necessary condition for stability is that the metric terms satisfy the following discrete GCL conditions:

$$(3.18) \quad \sum_{l=1}^3 \tilde{\mathbf{D}}_{\xi_l} \left[\mathcal{J} \frac{\partial \xi_l}{\partial x_m} \right] \tilde{\mathbf{i}} = \mathbf{0}.$$

Recognizing that $\tilde{\mathbf{D}}_{\xi_1}$ is not a tensor product operator, discrete metrics constructed using the analytic formalism of Vinokur and Yee [49] or Thomas and Lombard [48] will not in general satisfy the discrete GCL condition required in Eq. (3.18). The only viable alternative is to solve for discrete metrics that directly satisfy the GCL constraints.

Remark 3.4. Note that metric terms are assigned colors; e.g., the time-term Jacobian: \mathbf{J} or the volume metric terms: $\left[\mathcal{J} \frac{\partial \xi_l}{\partial x_m} \right]$. Metric terms with common colors form a clique and must be formed consistently. For example, the time-term Jacobian and the volume metric Jacobian need not be equivalent. Another important clique: the surface metrics, will be introduced in the next subsection.

3.3 Isolating the metrics The system (3.18) is a highly under-determined system which couples the approximation of the metrics in both elements. Worse still, whole clouds of nonconforming elements would in general need to be solved simultaneously, making the approach undesirable and even impracticable! A close examination of the volume terms provides insight on how to overcome this issue:

$$\begin{aligned}
& \tilde{\mathbf{P}} \left(\tilde{\mathbf{D}}_{\xi_1} \left[\mathcal{J} \frac{\partial \xi_1}{\partial x_m} \right] + \left[\mathcal{J} \frac{\partial \xi_1}{\partial x_m} \right] \tilde{\mathbf{D}}_{\xi_1} \right) = \\
& \begin{bmatrix} \mathbf{A}_{11} & \mathbf{A}_{12} \\ -\mathbf{A}_{12}^T & \mathbf{A}_{22} \end{bmatrix} + \left(\tilde{\mathbf{E}}_{\xi_1} \left[\mathcal{J} \frac{\partial \xi_1}{\partial x_m} \right] + \left[\mathcal{J} \frac{\partial \xi_1}{\partial x_m} \right] \tilde{\mathbf{E}}_{\xi_1} \right), \\
(3.19) \quad \mathbf{A}_{11} & \equiv \left\{ \mathbf{S}_{\xi_1}^L \left[\mathcal{J} \frac{\partial \xi_1}{\partial x_m} \right]_L + \left[\mathcal{J} \frac{\partial \xi_1}{\partial x_m} \right]_L \mathbf{S}_{\xi_1}^L \right\}, \\
\mathbf{A}_{12} & = \frac{1}{2} \left\{ \begin{array}{l} \left[\mathcal{J} \frac{\partial \xi_1}{\partial x_m} \right]_L \left(\mathbf{e}_{N_L} \mathbf{e}_{I_H}^T \otimes \mathbf{P}_L^{(1D)} \mathbf{I}_{HtoL}^{(1D)} \otimes \mathbf{P}_L^{(1D)} \mathbf{I}_{HtoL}^{(1D)} \right) \\ + \left(\mathbf{e}_{N_L} \mathbf{e}_{I_H}^T \otimes \mathbf{P}_L^{(1D)} \mathbf{I}_{HtoL}^{(1D)} \otimes \mathbf{P}_L^{(1D)} \mathbf{I}_{HtoL}^{(1D)} \right) \left[\mathcal{J} \frac{\partial \xi_1}{\partial x_m} \right]_H \end{array} \right\}, \\
\mathbf{A}_{22} & \equiv \left\{ \mathbf{S}_{\xi_1}^H \left[\mathcal{J} \frac{\partial \xi_1}{\partial x_m} \right]_H + \left[\mathcal{J} \frac{\partial \xi_1}{\partial x_m} \right]_H \mathbf{S}_{\xi_1}^H \right\}.
\end{aligned}$$

Replacing the highlighted off-diagonal metric terms in (3.19) with known metrics data, by construction preserves the skew-symmetry of the operator $\tilde{\mathbf{S}}_{\xi_i}$, but decouples the discrete GCL conditions (3.18). The highlighted off-diagonal surface metric terms: L and H become forcing data for the GCL condition. Note that L and H need not be equivalent, provided they are design order close.

Remark 3.5. More generally, \mathbf{A}_{12} can be composed of any terms that are design order interpolations from one element to the other and these can be constructed in a very general way, for example, one might consider first interpolating data to an intermediate set of Gauss nodes on which the metric terms are specified. The theoretical results in this paper apply to any such approach that is design order, satisfied the structural requirements presented above, and that uses specified metric information in the coupling terms.

With this approach, the discrete GCL conditions become (where contributions from the boundary SATs have been ignored)

$$\begin{aligned}
(3.20) \quad & 2\mathbf{P}^L \sum_{l=1}^3 \mathbf{D}_{\xi_l}^L \left[\mathcal{J} \frac{\partial \xi_l}{\partial x_m} \right]_L \mathbf{1}_L = \\
& \left\{ \left(\mathbf{e}_{N_L} \mathbf{e}_{N_L}^T \otimes \mathbf{P}_L^{(1D)} \otimes \mathbf{P}_L^{(1D)} \right) \left[\mathcal{J} \frac{\partial \xi_1}{\partial x_m} \right]_L + \left[\mathcal{J} \frac{\partial \xi_1}{\partial x_m} \right]_L \left(\mathbf{e}_{N_L} \mathbf{e}_{N_L}^T \otimes \mathbf{P}_L^{(1D)} \otimes \mathbf{P}_L^{(1D)} \right) \right\} \mathbf{1}_L \\
& - \left\{ \left(\mathbf{e}_{N_L} \otimes \mathbf{I}_{N_L} \otimes \mathbf{I}_{N_L} \right) \left[\mathcal{J} \frac{\partial \xi_1}{\partial x_m} \right]_L^{\hat{\Gamma}} \left(\mathbf{P}_L^{(1D)} \mathbf{I}_{HtoL}^{(1D)} \otimes \mathbf{P}_L^{(1D)} \mathbf{I}_{HtoL}^{(1D)} \right) \left(\mathbf{e}_{I_H}^T \otimes \mathbf{I}_{N_H} \otimes \mathbf{I}_{N_H} \right) \right\} \mathbf{1}_H \\
& - \left\{ \left(\mathbf{e}_{N_L} \otimes \mathbf{I}_{N_L} \otimes \mathbf{I}_{N_L} \right) \left(\mathbf{P}_L^{(1D)} \mathbf{I}_{HtoL}^{(1D)} \otimes \mathbf{P}_L^{(1D)} \mathbf{I}_{HtoL}^{(1D)} \right) \left[\mathcal{J} \frac{\partial \xi_1}{\partial x_m} \right]_H^{\hat{\Gamma}} \left(\mathbf{e}_{I_H}^T \otimes \mathbf{I}_{N_H} \otimes \mathbf{I}_{N_H} \right) \right\} \mathbf{1}_H,
\end{aligned}$$

(3.21)

$$\begin{aligned}
2\mathbb{P}^L \sum_{l=1}^3 \mathbb{D}_{\xi_l}^H \left[\mathcal{J} \frac{\partial \xi_l}{\partial x_m} \right]_H \mathbf{1}_H = & \\
- \left\{ \left(\mathbf{e}_{1_H} \mathbf{e}_{1_H}^T \otimes \mathbb{P}_H^{(1D)} \otimes \mathbb{P}_H^{(1D)} \right) \left[\mathcal{J} \frac{\partial \xi_1}{\partial x_m} \right]_H + \left[\mathcal{J} \frac{\partial \xi_1}{\partial x_m} \right]_H \left(\mathbf{e}_{1_L} \mathbf{e}_{1_H}^T \otimes \mathbb{P}_H^{(1D)} \otimes \mathbb{P}_H^{(1D)} \right) \right\} \mathbf{1}_H & \\
+ \left\{ \left(\mathbf{e}_{1_H} \otimes \mathbb{I}_{N_H} \otimes \mathbb{I}_{N_L} \right) \left[\mathcal{J} \frac{\partial \xi_1}{\partial x_m} \right]_H^{\hat{\Gamma}} \left(\mathbb{P}_H^{(1D)} \mathbb{I}_{LtoH}^{(1D)} \otimes \mathbb{P}_H^{(1D)} \mathbb{I}_{LtoH}^{(1D)} \right) \left(\mathbf{e}_{N_L}^T \otimes \mathbb{I}_{N_L} \otimes \mathbb{I}_{N_L} \right) \right\} \mathbf{1}_L & \\
+ \left\{ \left(\mathbf{e}_{1_H} \otimes \mathbb{I}_{N_H} \otimes \mathbb{I}_{N_H} \right) \left(\mathbb{P}_H^{(1D)} \mathbb{I}_{LtoH}^{(1D)} \otimes \mathbb{P}_H^{(1D)} \mathbb{I}_{LtoH}^{(1D)} \right) \left[\mathcal{J} \frac{\partial \xi_1}{\partial x_m} \right]_L^{\hat{\Gamma}} \left(\mathbf{e}_{N_L}^T \otimes \mathbb{I}_{N_L} \otimes \mathbb{I}_{N_L} \right) \right\} \mathbf{1}_L. &
\end{aligned}$$

The matrix $\left[\mathcal{J} \frac{\partial \xi_1}{\partial x_m} \right]_L^{\hat{\Gamma}}$ is of size $N_L^2 \times N_L^2$ (N_L is the number of nodes in each computational direction on element L) and its diagonal elements are approximations to the metrics on the surface nodes of element L at the shared interface. An analogous definition holds for $\left[\mathcal{J} \frac{\partial \xi_1}{\partial x_m} \right]_H^{\hat{\Gamma}}$. In order to decouple the two systems of equations in (3.20) and (3.21) the terms in $\left[\mathcal{J} \frac{\partial \xi_1}{\partial x_m} \right]_L^{\hat{\Gamma}}$ and $\left[\mathcal{J} \frac{\partial \xi_1}{\partial x_m} \right]_H^{\hat{\Gamma}}$ need to be specified, for example, using the analytic metrics, which is the approach used in this paper. For later use, we introduce notation for the macro element $\tilde{\mathbb{D}}_{l,m}$ which is the macro element operator constructed as described above for the metric terms $\mathcal{J}_\kappa \frac{\partial \xi_l}{\partial x_m}$.

The next section details how to construct the metrics so that the remaining discrete GCL conditions are satisfied.

3.4 Metric solution mechanics In this section, to demonstrate the proposed approach for approximating the metric terms, the discrete GCL conditions associated with the element L (3.20) are used.

Note that for an arbitrary interior element, the discrete GCL system that needs to be solved includes the coupling terms on all six faces, while for the simplified problem considered above only the (nonconforming) coupling on the vertical interface appears.

Eq. (3.20) can be algebraically manipulated into a form that is more convenient for constructing a solution procedure for the metric terms. This form is derived by multiplying Eq. (3.20) by -1 , using the SBP property $\mathbb{Q}_L^{(1D)} = -\left(\mathbb{Q}_L^{(1D)}\right)^T + \mathbb{E}_L^{(1D)}$, and canceling common terms. Doing so results in

(3.22)

$$\begin{aligned}
2 \sum_{l=1}^3 \left(\mathbb{Q}_{\xi_l}^L\right)^T \left[\mathcal{J} \frac{\partial \xi_l}{\partial x_m} \right]_L \mathbf{1}_L = & \\
- \left\{ \left(\mathbf{e}_{N_L} \otimes \mathbb{I}_{N_L} \otimes \mathbb{I}_{N_L} \right) \left[\mathcal{J} \frac{\partial \xi_1}{\partial x_m} \right]_L^{\hat{\Gamma}} \left(\mathbb{P}_L^{(1D)} \mathbb{I}_{HtoL}^{(1D)} \otimes \mathbb{P}_L^{(1D)} \mathbb{I}_{HtoL}^{(1D)} \right) \left(\mathbf{e}_{1_H}^T \otimes \mathbb{I}_{N_H} \otimes \mathbb{I}_{N_H} \right) \right\} \mathbf{1}_H & \\
- \left\{ \left(\mathbf{e}_{N_L} \otimes \mathbb{I}_{N_L} \otimes \mathbb{I}_{N_L} \right) \left(\mathbb{P}_L^{(1D)} \mathbb{I}_{HtoL}^{(1D)} \otimes \mathbb{P}_L^{(1D)} \mathbb{I}_{HtoL}^{(1D)} \right) \left[\mathcal{J} \frac{\partial \xi_1}{\partial x_m} \right]_H^{\hat{\Gamma}} \left(\mathbf{e}_{1_H}^T \otimes \mathbb{I}_{N_H} \otimes \mathbb{I}_{N_H} \right) \right\} \mathbf{1}_H, &
\end{aligned}$$

$m = 1, 2, 3$,

where $\mathbb{Q}_{\xi_1}^L \equiv \mathbb{Q}_L^{(1D)} \otimes \mathbb{P}_L^{(1D)} \otimes \mathbb{P}_L^{(1D)}$, $\mathbb{Q}_{\xi_2}^L \equiv \mathbb{P}_L^{(1D)} \otimes \mathbb{Q}_L^{(1D)} \otimes \mathbb{P}_L^{(1D)}$, $\mathbb{Q}_{\xi_3}^L \equiv \mathbb{P}_L^{(1D)} \otimes$

$\mathbf{P}_L^{(1D)} \otimes \mathbf{Q}_L^{(1D)}$. Note that the contributions from the \mathbf{E}_{ξ_i} from the left-hand side (i.e., coming from the step $\mathbf{Q} = -\mathbf{Q}^T + \mathbf{E}$) related to the boundaries of the macro element are ignored. These contributions interact with the boundary SATs in the same way as the interface does.

The metric terms in Eq. (3.22) are determined by solving a strictly convex quadratic optimization problem, following the algorithm given in Crean *et al.* [11]:

$$(3.23) \quad \min_{\mathbf{a}_m} \frac{1}{2} (\mathbf{a}_m^L - \mathbf{a}_{m,\text{target}}^L)^T (\mathbf{a}_m^L - \mathbf{a}_{m,\text{target}}^L), \quad \text{subject to} \quad \mathbf{M}^L \mathbf{a}_m^L = \mathbf{c}_m^L, \\ m = 1, 2, 3,$$

where \mathbf{a}_m^L and $\mathbf{a}_{m,\text{target}}^L$ are the optimized and targeted metric terms, respectively, and

$$(\mathbf{a}_m^L)^T \equiv \mathbf{1}_L^T \left[\left[\mathcal{J} \frac{\partial \xi_1}{\partial x_m} \right]_L, \left[\mathcal{J} \frac{\partial \xi_2}{\partial x_m} \right]_L, \left[\mathcal{J} \frac{\partial \xi_3}{\partial x_m} \right]_L \right], \quad \mathbf{M}^L \equiv \left[(\mathbf{Q}_{\xi_1}^L)^T, (\mathbf{Q}_{\xi_2}^L)^T, (\mathbf{Q}_{\xi_3}^L)^T \right], \\ 2\mathbf{c}_m^L \equiv \\ - \left\{ (\mathbf{e}_{N_L} \otimes \mathbf{l}_{N_L} \otimes \mathbf{l}_{N_L}) \left[\mathcal{J} \frac{\partial \xi_1}{\partial x_m} \right]_L^{\hat{\Gamma}} \left(\mathbf{P}_L^{(1D)} \mathbf{l}_{\text{HtoL}}^{(1D)} \otimes \mathbf{P}_L^{(1D)} \mathbf{l}_{\text{HtoL}}^{(1D)} \right) (\mathbf{e}_{\mathbf{I}_H}^T \otimes \mathbf{l}_{N_H} \otimes \mathbf{l}_{N_H}) \right\} \mathbf{1}_H \\ - \left\{ (\mathbf{e}_{N_L} \otimes \mathbf{l}_{N_L} \otimes \mathbf{l}_{N_L}) \left(\mathbf{P}_L^{(1D)} \mathbf{l}_{\text{HtoL}}^{(1D)} \otimes \mathbf{P}_L^{(1D)} \mathbf{l}_{\text{HtoL}}^{(1D)} \right) \left[\mathcal{J} \frac{\partial \xi_1}{\partial x_m} \right]_H^{\hat{\Gamma}} (\mathbf{e}_{\mathbf{I}_H}^T \otimes \mathbf{l}_{N_H} \otimes \mathbf{l}_{N_H}) \right\} \mathbf{1}_H,$$

with \mathbf{a}_m^L of size $3(N_L)^3 \times 1$, \mathbf{M}^L of size $(N_L)^3 \times 3(N_L)^3$ and \mathbf{c}_m^L of size $(N_L)^3 \times 1$. The optimal solution, in the Cartesian 2-norm, is given by (see Proposition 1 in Crean *et al.* [11])

$$(3.24) \quad \mathbf{a}_m^L = \mathbf{a}_{m,\text{target}}^L - (\mathbf{M}^L)^\dagger (\mathbf{M}^L \mathbf{a}_{m,\text{target}}^L - \mathbf{c}_m^L),$$

with $(\mathbf{M}^L)^\dagger$ the Moore-Penrose pseudo-inverse of \mathbf{M}^L . The pseudo-inverse is computed using a singular value decomposition (SVD) of \mathbf{M}^L

$$\mathbf{M}^L = \mathbf{U}^L \Sigma^L (\mathbf{V}^L)^T, \quad (\mathbf{M}^L)^\dagger = \mathbf{V}^L (\Sigma^L)^\dagger (\mathbf{U}^L)^T,$$

with \mathbf{U}^L an $(N_L)^3 \times (N_L)^3$ unitary matrix, Σ^L an $(N_L)^3 \times (N_L)^3$ diagonal matrix containing the singular values of \mathbf{M}^L , and $(\mathbf{V}^L)^T$ an $(N_L)^3 \times 3(N_L)^3$ matrix with orthonormal rows. Although the solution (\mathbf{a}_m^L given by Eq. (3.24)) is optimal, it is not guaranteed to **exactly** satisfy Eq. (3.23) (i.e., machine precision). The following theorem establishes an additional constrain on the surface metrics.

THEOREM 1. *The surface metrics, \mathbf{c}_m^L , must satisfy the additional constraint*

$$(3.25) \quad \mathbf{1}_L^T \mathbf{c}_m^L = 0,$$

to guarantee an exact solution of the discrete GCL condition given in Eq. (3.23).

Proof. The matrix \mathbf{M}^L is constructed from the transposes of three derivative operators: $(\mathbf{D}_{\xi_i}^L)^T \mathbf{P}^L = (\mathbf{Q}_{\xi_i}^L)^T$, with the constant vector $\mathbf{1}_L$, in its null space, i.e., $\mathbf{1}_L^T (\mathbf{Q}_{\xi_i}^L)^T = \mathbf{0}^T$. Thus, the matrix \mathbf{M}^L has a row rank of $(N_L)^3 - 1$ and one zero singular value.

Assemble the singular values in the diagonal matrix (Σ^L) in descending order.

This implies that i) the final singular value is zero, $\Sigma((N_L)^3, (N_L)^3) = 0$, ii) the final orthonormal column vector in \mathbf{U}^L is a constant multiple of the vector, $\mathbf{1}_L$, and iii) the pseudo-inverse is given by $(\Sigma^L)^\dagger(i, i) = \frac{1}{\Sigma^L(i, i)}$, $i = 1, \dots, (N_L)^3 - 1$.

The optimal solution given in Eq. (3.24) can thus be expressed as

$$\mathbf{a}_m^L = \mathbf{a}_{m,\text{target}}^L - \mathbf{V}^L (\Sigma^L)^\dagger \left(\Sigma^L (\mathbf{V}^L)^\top \mathbf{a}_{m,\text{target}}^L - (\mathbf{U}^L)^\top \mathbf{c}_m^L \right).$$

Since the diagonal matrices $(\Sigma^L)^\dagger$ and Σ^L are rank deficient in their $((N_L)^3, (N_L)^3)$ positions, a zero solution exists only if the final constant vector, dotted with the metric data is zero, i.e., $(\mathbf{U}^L)^\top \mathbf{c}_m^L = \mathbf{1}_L^\top \mathbf{c}_m^L = 0$. The proof is established. \square

Inspection of the definition for \mathbf{c}_m^L given in Eq. (3.25), reveals that the constraint $\mathbf{1}_L^\top \mathbf{c}_m^L = 0$, may be interpreted as the discrete integral of surface metric data. This integral must be zero as is motivated by the following derivation.

Integrate the continuous GCL equations over the domain $\hat{\Omega}_L$, and apply Gauss' divergence theorem to the integral. The resulting expressions are

$$\int_{\hat{\Omega}_L} \sum_{l=1}^3 \frac{\partial}{\partial \xi_l} \left(\mathcal{J} \frac{\partial \xi_l}{\partial x_m} \right) d\hat{\Omega}_L = \oint_{\hat{\Gamma}_L} \sum_{l=1}^3 \left(\mathcal{J} \frac{\partial \xi_l}{\partial x_m} \right) n_{\xi_l} d\hat{\Gamma}_L \approx \mathbf{1}_L^\top \mathbf{c}_m^L = 0.$$

Thus, the constraint $\mathbf{1}_L^\top \mathbf{c}_m^L = 0$ is the discrete surface metric equivalent of the analytic surface integral consistency constraint.

There are at least two convenient ways of enforcing this constraint: 1) polynomially exact (analytic) surface metrics or 2) metrics constructed using conventional FD approaches [49, 48]. The adequacy of these approaches is demonstrated by a careful investigation of the surface metrics arising from tensor-product transformations.

Consider a degree p tensor-product curvilinear coordinate transformation. The surface metrics and the coupling terms constructed on the joint surface are of degree $2p - 1$ in the surface orthogonal directions. Thus, a surface mass matrix with quadrature strength $2p - 1$, (e.g., LGL) integrates the surface terms exactly and immediately satisfies the constraint: $\mathbf{1}_L^\top \mathbf{c}_m^L = 0$. The following theorem establishes that the resulting coupling terms satisfy the required integral constraints.

THEOREM 2. *The coupling terms constructed on a conforming face between a conforming element and an element that has at least one other face that is nonconforming satisfy the condition (3.25) if either 1) analytic or 2) standard FD approaches (e.g., Vinokur and Yee [49] or Thomas and Lombard), are used to seed the metric terms.*

Proof. This proof follows by inserting the approximation of the metric terms using 1) analytic, or 2) either Vinokur or Yee [49] or Thomas and Lombard [48], and the polynomial exactness of the differentiation matrices and the norm matrices (the details of the proof are given in Appendix G. [15]). \square

Remark 3.6. The 1) GCL optimized volume metrics on all faces of a nonconforming element, and the 2) surface metrics specified in the coupling matrices, are both surface normal approximations but in general differ by a design order term. They are weakly coupled through the GCL constraint given in equation (3.22).

The following theorem summarizes the properties of the proposed coupling approach.

THEOREM 3. *The proposed coupling procedure results in a scheme that has the following properties:*

- *The scheme is discretely entropy conservative (i.e., neutral discrete L^2 sta-*

bility under the assumption of positive temperature and density)

- The scheme is discretely elementwise conservative and preserves freestream
- The scheme is of order $p_L + d - 1$ where p_L is the lowest degree used (the $+d$ comes from the fact that the PDE and therefore the discretization have been multiplied by the metric Jacobian which scales as h^d)

Proof. The proof of entropy conservation is given in Section (5.2) while appropriate interface dissipation leading to entropy stability is discussed in Section 6. Elementwise conservation is proven in Appendix E in [15]. The order of the scheme results from the fact that one of the interpolation operators is suboptimal ($p_L - 1$). \square

4 Nonlinearly stable schemes: Burgers' equation The nonconforming interface coupling mechanics presented in the previous section will be generalized for the compressible Euler equations in Section 5. Proving stability of nonlinear conservation laws, in general requires elaborate techniques well beyond simply discretizing the derivatives of the fluxes directly with SBP operators. Next, the Hadamard derivative formalize is introduced in the context of one-dimensional inviscid Burgers' equation, which has the desirable property of being amenable to either 1) a canonical derivative splitting, or 2) the Hadamard derivative approach. The equivalence between the two approaches for Burgers' equation, is established elsewhere [21, 6].

Inviscid Burgers' equation and its well-known canonical splitting are of the form

$$(4.1) \quad \frac{\partial \mathcal{U}}{\partial t} + \frac{\partial}{\partial x_1} \left(\frac{\mathcal{U}^2}{2} \right) = 0 \quad ; \quad \frac{\partial \mathcal{U}}{\partial t} + \frac{1}{3} \frac{\partial}{\partial x_1} (\mathcal{U}^2) + \frac{\mathcal{U}}{3} \frac{\partial \mathcal{U}}{\partial x_1} = 0.$$

Performing an energy analysis on the split form of (4.1) gives (see, for instance, [6] for details)

$$(4.2) \quad \frac{1}{2} \frac{d \|\mathcal{U}\|^2}{dt} + \oint_{\Gamma} \frac{\mathcal{U}^3}{3} n_{x_1} d\Gamma = 0, \quad \|\mathcal{U}\|^2 \equiv \int_{\Omega} \mathcal{U}^2 d\Omega.$$

In order to prove stability, the semi-discrete scheme needs to mimic (4.2) in the sense that when contracted with $\mathbf{u}^T \mathbf{P}$ (the discrete analogue of multiplying by the solution and integrating in space) the result is given by the sum of spatial terms that telescope to the boundaries.

The discretization of (4.1) with SBP operators (ignoring the SATs) is given as

$$(4.3) \quad \frac{d\mathbf{u}}{dt} + \frac{1}{3} \mathbf{D}_{x_1} \text{diag}(\mathbf{u}) \mathbf{u} + \frac{1}{3} \text{diag}(\mathbf{u}) \mathbf{D}_{x_1} \mathbf{u} = 0.$$

Multiplying (4.3) by $\mathbf{u}^T \mathbf{P}$ results in

$$(4.4) \quad \frac{1}{2} \frac{d \mathbf{u}^T \mathbf{P} \mathbf{u}}{dt} + \frac{1}{3} (\mathbf{u}^3(N) - \mathbf{u}^3(1)) = 0,$$

for which each term mimics (4.2) and has the telescoping property, i.e., what remains are terms at the boundaries.

Now the discretization (4.3) is recast using the Hadamard derivative formalism. The Hadamard derivative operator and the equivalent split form operators are given as follows

$$(4.5) \quad 2\mathbf{D}_{x_1} \circ \mathbf{F}_{x_1}(\mathbf{u}, \mathbf{u}) \mathbf{1}_1 \quad \leftrightarrow \quad \frac{1}{3} \mathbf{D}_{x_1} \text{diag}(\mathbf{u}) \mathbf{u} + \frac{1}{3} \text{diag}(\mathbf{u}) \mathbf{D}_{x_1} \mathbf{u}.$$

The Hadamard operator is capable of compactly representing various split forms, and more importantly, extends to nonlinear equations for which a canonical split form is inappropriate.

The Hadamard derivative operator is constructed from two components: 1) an SBP derivative operator, and 2) a two point flux function specific to the physics being

modeled. Two point fluxes are constructed between the center point and all other points of dependency within the SBP stencil. The SBP telescoping property [21] that results from precise local cancellation of spatial terms, can then be extended directly to nonlinear operators. A simple example is now presented.

Consider the two point Burgers' flux function defined by [47, 6]

$$\mathbf{f}_{x_m}^{sc}(\mathbf{u}^{(i)}, \mathbf{u}^{(j)}) \equiv \frac{\left\{ (\mathbf{u}^{(i)})^2 + \mathbf{u}^{(i)}\mathbf{u}^{(j)} + (\mathbf{u}^{(j)})^2 \right\}}{6},$$

where $\mathbf{u}^{(i)}$ and $\mathbf{u}^{(j)}$ are the i^{th} and j^{th} components of \mathbf{u} , and for the purpose of demonstration, a simple SBP operator constructed on the LGL nodes $(-1, 0, 1)$

$$\mathbf{D}_{x_1} = \begin{bmatrix} -\frac{3}{2} & 2 & -\frac{1}{2} \\ -\frac{1}{2} & 0 & \frac{1}{2} \\ \frac{1}{2} & -2 & \frac{3}{2} \end{bmatrix}.$$

The two argument Hadamard matrix flux, $\mathbf{F}_{x_m}(\mathbf{u}, \mathbf{u})$ is given as

$$\mathbf{F}_{x_m}(\mathbf{u}, \mathbf{u}) = \begin{bmatrix} \frac{(\mathbf{u}^{(1)})^2}{2} & \frac{(\mathbf{u}^{(1)})^2 + \mathbf{u}^{(1)}\mathbf{u}^{(2)} + (\mathbf{u}^{(2)})^2}{6} & \frac{(\mathbf{u}^{(1)})^2 + \mathbf{u}^{(1)}\mathbf{u}^{(3)} + (\mathbf{u}^{(3)})^2}{6} \\ \frac{(\mathbf{u}^{(2)})^2 + \mathbf{u}^{(2)}\mathbf{u}^{(1)} + (\mathbf{u}^{(1)})^2}{6} & \frac{(\mathbf{u}^{(2)})^2}{2} & \frac{(\mathbf{u}^{(2)})^2 + \mathbf{u}^{(2)}\mathbf{u}^{(3)} + (\mathbf{u}^{(3)})^2}{6} \\ \frac{(\mathbf{u}^{(3)})^2 + \mathbf{u}^{(3)}\mathbf{u}^{(1)} + (\mathbf{u}^{(1)})^2}{6} & \frac{(\mathbf{u}^{(3)})^2 + \mathbf{u}^{(3)}\mathbf{u}^{(2)} + (\mathbf{u}^{(2)})^2}{6} & \frac{(\mathbf{u}^{(3)})^2}{2} \end{bmatrix}.$$

Thus,

$$\mathbf{D}_{x_1} \circ \mathbf{F}_{x_m}(\mathbf{u}, \mathbf{u}) \mathbf{1} = \begin{bmatrix} -\frac{3}{2} \frac{(\mathbf{u}^{(1)})^2}{2} & \frac{(\mathbf{u}^{(1)})^2 + \mathbf{u}^{(1)}\mathbf{u}^{(2)} + (\mathbf{u}^{(2)})^2}{6} & -\frac{1}{2} \frac{(\mathbf{u}^{(1)})^2 + \mathbf{u}^{(1)}\mathbf{u}^{(3)} + (\mathbf{u}^{(3)})^2}{6} \\ -\frac{1}{2} \frac{(\mathbf{u}^{(2)})^2 + \mathbf{u}^{(2)}\mathbf{u}^{(1)} + (\mathbf{u}^{(1)})^2}{6} & 0 & \frac{1}{2} \frac{(\mathbf{u}^{(2)})^2 + \mathbf{u}^{(2)}\mathbf{u}^{(3)} + (\mathbf{u}^{(3)})^2}{6} \\ \frac{1}{2} \frac{(\mathbf{u}^{(3)})^2 + \mathbf{u}^{(3)}\mathbf{u}^{(1)} + (\mathbf{u}^{(1)})^2}{6} & -2 \frac{(\mathbf{u}^{(3)})^2 + \mathbf{u}^{(3)}\mathbf{u}^{(2)} + (\mathbf{u}^{(2)})^2}{6} & \frac{3}{2} \frac{(\mathbf{u}^{(3)})^2}{2} \end{bmatrix} \begin{bmatrix} 1 \\ 1 \\ 1 \end{bmatrix}.$$

The equivalence between the two approaches is evident by inspection.

Now the general notation applicable to the compressible Euler equations is described. Assume that what is required is the discretization of the derivative of a flux vector \mathcal{F}_{x_m} in the x_m Cartesian direction. The essential ingredients used above are an SBP matrix difference operator, \mathbf{D}_{x_m} , and a two argument matrix flux function, $\mathbf{F}_{x_m}(\mathbf{u}_\kappa, \mathbf{u}_r)$, which is composed of diagonal matrices and is defined block-wise as

$$(\mathbf{F}_{x_m}(\mathbf{u}_\kappa, \mathbf{u}_r))(e(i-1)+1 : ei, e(j-1)+1 : ej) \equiv \text{diag} \left(\mathbf{f}_{x_m}^{sc}(\mathbf{u}_\kappa^{(i)}, \mathbf{u}_r^{(j)}) \right),$$

$$\mathbf{u}_\kappa^{(i)} \equiv \mathbf{u}_\kappa(e(i-1)+1 : ei), \quad \mathbf{u}_r^{(j)} \equiv \mathbf{u}_r(e(j-1)+1 : ej),$$

$$i = 1 \dots, N_\kappa^3, \quad j = 1, \dots, N_r^3,$$

where e is the number of equations in the system of PDEs. For example, for the compressible Euler equations, $e = 5$ and the two argument matrix flux function is of size $(eN_\kappa^3) \times (eN_r^3)$, where eN_κ^3 and eN_r^3 are the total number of entries in the vectors \mathbf{u}_κ

and \mathbf{u}_r corresponding the solution variables in elements κ and r , respectively. Thus, $\mathbf{u}_\kappa^{(i)}$ is the vector of the e solution variables evaluated at the i^{th} node. The vectors $\mathbf{f}_{x_m}^{sc}(\mathbf{u}_\kappa^{(i)}, \mathbf{u}_r^{(j)})$ are constructed from two-point flux functions that are symmetric in their arguments, $(\mathbf{u}_\kappa^{(i)}, \mathbf{u}_r^{(j)})$, and consistent. Thus,

$$\mathbf{f}_{x_m}^{sc}(\mathbf{u}_\kappa^{(i)}, \mathbf{u}_r^{(j)}) = \mathbf{f}_{x_m}^{sc}(\mathbf{u}_r^{(j)}, \mathbf{u}_\kappa^{(i)}), \quad \mathbf{f}_{x_m}^{sc}(\mathbf{u}_\kappa^{(i)}, \mathbf{u}_\kappa^{(i)}) = \mathcal{F}_{x_m}(\mathbf{u}_\kappa^{(i)}),$$

where \mathcal{F}_{x_m} is the flux vector in the x_m^{th} Cartesian direction. Using these ingredients, an approximation to the derivative $\frac{\partial \mathcal{F}_{x_m}}{\partial x_m}$ is constructed as

$$2D_{x_m} \circ F_{x_m}(\mathbf{q}_\kappa, \mathbf{q}_\kappa) \mathbf{1}_\kappa \approx \frac{\partial \mathcal{F}_{x_m}}{\partial x_m}(\boldsymbol{\xi}^\kappa),$$

where $\boldsymbol{\xi}^\kappa$ is the vector of vectors containing the nodal locations. The resulting approximation has the same order properties as differentiating directly with the SBP operator D_{x_m} (see Theorem 1 in Crean *et al.* [11]).

5 Application to the compressible Euler equations In this section, the non-conforming algorithm presented in Section 3 is combined with the mechanics presented in Section 4 to construct an entropy conservative discretization of the compressible Euler equations on p -nonconforming meshes. First, in Section 5.1 the continuous equations and the continuous entropy analysis are reviewed, then in Section 5.2 the semi-discrete algorithm for the Euler equations is presented and analyzed.

5.1 Review of the continuous entropy analysis The strong form of the compressible Euler equations in Cartesian coordinates are given as

$$(5.1) \quad \begin{aligned} \frac{\partial \mathcal{Q}}{\partial t} + \sum_{m=1}^3 \frac{\partial \mathcal{F}_{x_m}}{\partial x_m} &= 0, & \forall (x_1, x_2, x_3) \in \Omega, \quad t \geq 0, \\ \mathcal{Q}(x_1, x_2, x_3, t) &= \mathcal{G}^{(B)}(x_1, x_2, x_3, t), & \forall (x_1, x_2, x_3) \in \Gamma, \quad t \geq 0, \\ \mathcal{Q}(x_1, x_2, x_3, 0) &= \mathcal{G}^{(0)}(x_1, x_2, x_3, 0), & \forall (x_1, x_2, x_3) \in \Omega. \end{aligned}$$

The vectors \mathcal{Q} and \mathcal{F}_x respectively denote the conserved variables and the inviscid fluxes. The boundary data, $\mathcal{G}^{(B)}$, and the initial condition, $\mathcal{G}^{(0)}$, are assumed to be in $L^2(\Omega)$, with the further assumption that $\mathcal{G}^{(B)}$ will be set to coincide with linear well-posed boundary conditions and such that entropy conservation or stability is achieved.

It is well-known that the compressible Euler equations (5.1) possess a convex extension that, when integrated over the physical domain Ω , only depends on the boundary data on Γ . Such an extension yields the entropy function

$$(5.2) \quad \mathcal{S} = -\rho s,$$

where ρ and s are the density and the thermodynamic entropy, respectively. The entropy function, \mathcal{S} , is convex if the thermodynamic variables are positive and is a useful tool for proving stability in the L^2 norm [12]. Following the analysis described in [3, 35, 7], the system (5.1) is multiplied by the (local) entropy variables $\mathcal{W}^T = \partial \mathcal{S} / \partial \mathcal{Q}$ and by using the fact that

$$(5.3) \quad \frac{\partial \mathcal{S}}{\partial \mathcal{Q}} \frac{\partial \mathcal{F}_{x_m}}{\partial x_m} = \frac{\partial \mathcal{S}}{\partial \mathcal{Q}} \frac{\partial \mathcal{F}_{x_m}}{\partial \mathcal{Q}} \frac{\partial \mathcal{Q}}{\partial x_m} = \frac{\partial \mathcal{F}_{x_m}}{\partial \mathcal{Q}} \frac{\partial \mathcal{Q}}{\partial x_m} = \frac{\partial \mathcal{F}_{x_m}}{\partial x_m}, \quad m = 1, 2, 3,$$

gives that

$$(5.4) \quad \frac{\partial \mathcal{S}}{\partial t} + \sum_{m=1}^3 \frac{\partial \mathcal{F}_{x_m}}{\partial x_m} = 0,$$

where the scalars $\mathcal{F}_{x_m}(\mathcal{Q})$ are the entropy fluxes in the x_m -direction. Then, integrating over the domain, Ω , and using integration by parts yields

$$(5.5) \quad \int_{\Omega} \frac{\partial \mathcal{S}}{\partial t} d\Omega \leq \oint_{\Gamma} \left(\sum_{m=1}^3 \mathcal{F}_{x_m} n_{x_m} \right) d\Omega,$$

where n_{x_m} is the m^{th} component of the outward facing unit normal. Note that the equality in (5.5) holds for smooth flows; conversely, the inequality is valid for non smooth flow since the mathematical entropy decreases across shocks.

To obtain a bound on the solution, the inequality (5.5) is integrated in time and assuming boundary conditions and an initial condition that are nonlinearly well posed, and positivity of density and temperature, the result can be turned into a bound on the solution in terms of the data of the problem (see [42, 12]). Example of fully-discrete explicit entropy conservative/stable algorithms are presented, for instance, in [23, 36].

5.2 A p -nonconforming algorithm As for the convection equation, a skew-symmetrically split form of the compressible Euler equations is used to construct an entropy conservative/stable algorithm:

$$(5.6) \quad \begin{aligned} & \mathcal{J}_{\kappa} \frac{\partial \mathcal{Q}_{\kappa}}{\partial t} + \sum_{l,m=1}^3 \frac{1}{2} \left\{ \frac{\partial}{\partial \xi_l} \left(\mathcal{J}_{\kappa} \frac{\partial \xi_l}{\partial x_m} \mathcal{F}_{x_m} \right) + \mathcal{J}_{\kappa} \frac{\partial \xi_l}{\partial x_m} \frac{\partial \mathcal{F}_{x_m}}{\partial \xi_l} \right\} \\ & - \frac{1}{2} \sum_{l,m=1}^3 \mathcal{F}_{x_m} \frac{\partial}{\partial \xi_l} \left(\mathcal{J}_{\kappa} \frac{\partial \xi_l}{\partial x_m} \right) = 0, \end{aligned}$$

where the last term on the left-hand side is zero as a result of the GCL conditions (3.6).

The discretization is developed using the same macro element SBP operator as in Section 3. Thus, the discretization of (5.6) over the macro element is given as

$$(5.7) \quad \mathcal{J} \frac{d\tilde{\mathbf{q}}}{dt} + \sum_{l,m=1}^3 \tilde{\mathbf{D}}_{l,m} \circ \mathbf{F}_{x_m}(\tilde{\mathbf{q}}, \tilde{\mathbf{q}}) \tilde{\mathbf{1}} - \frac{1}{2} \sum_{l,m=1}^3 \text{diag}(\mathbf{f}_{x_m}) \tilde{\mathbf{D}}_{\xi_l} \left[\mathcal{J} \frac{\partial \xi_l}{\partial x_m} \right] \tilde{\mathbf{1}} = \mathbf{0},$$

$$\tilde{\mathbf{q}} \equiv [\mathbf{q}_L^T, \mathbf{q}_H^T]^T,$$

where \mathbf{f}_{x_m} is a vector of vectors constructed by evaluating \mathcal{F}_{x_m} at the mesh nodes. That the factor of $\frac{1}{2}$ on the skew-symmetric volume terms disappears as a result of using the nonlinear operator, e.g., $2\mathbf{D}_{\xi_l} \circ \mathbf{F}_{x_m}(\mathbf{q}_{\kappa}, \mathbf{q}_{\kappa}) \mathbf{1}_{\kappa} \approx \frac{\partial \mathcal{F}_{x_m}}{\partial \xi_l}(\boldsymbol{\xi}^{\kappa})$. Moreover, the flux function matrix, $\mathbf{F}_{x_m}(\tilde{\mathbf{q}}, \tilde{\mathbf{q}})$, is constructed using a two point flux function, $\mathbf{f}_{x_m}^{sc}(\tilde{\mathbf{q}}^{(i)}, \tilde{\mathbf{q}}^{(j)})$, that satisfies the Tadmor shuffle condition [47]

$$(5.8) \quad \left(\tilde{\mathbf{w}}^{(i)} - \tilde{\mathbf{w}}^{(j)} \right)^T \mathbf{f}_{x_m}^{sc}(\tilde{\mathbf{q}}^{(i)}, \tilde{\mathbf{q}}^{(j)}) = \tilde{\psi}_{x_m}^{(i)} - \tilde{\psi}_{x_m}^{(j)}.$$

The $\tilde{\mathbf{D}}_{l,m}$ operators are constructed as in Section (3) by tensoring the contributing matrices with an identity matrix \mathbf{I}_5 to accommodate the system of 5 equations. For example,

$$\mathbf{D}_{\xi_1}^L \equiv \bar{\mathbf{D}}_{\xi_1} \otimes \mathbf{I}_5, \quad \bar{\mathbf{D}}_{\xi_1}^L \equiv \mathbf{D}_L^{(1D)} \otimes \mathbf{I}_{N_L} \otimes \mathbf{I}_{N_L}.$$

Nonlinear stability requires that the last set of terms on the left-hand side of (5.7)

be zero. This requirement leads to discrete GCL conditions which are identical to those obtained for the convection equation (with D_{ξ_l} replaced with \bar{D}_{ξ_l}), i.e., conditions (3.20) and (3.21).

The procedure to demonstrate that the proposed scheme is entropy conservative (i.e., it telescopes to the element boundaries) follows the continuous analysis in a one-to-one fashion (see Section 5.1). To simplify the derivation, the following matrices are introduced:

$$\hat{D}_m \equiv \sum_{l=1}^3 \tilde{D}_{l,m}, \quad \hat{Q}_m \equiv \tilde{P} \hat{D}_m, \quad \hat{E}_m \equiv \hat{Q}_m + \hat{Q}_m^T.$$

Thus, assuming that the discrete GCL conditions are satisfied, (5.7) becomes

$$(5.9) \quad \mathcal{J} \frac{d\tilde{\mathbf{q}}}{dt} + \sum_{m=1}^3 \hat{D}_m \circ F_{x_m}(\tilde{\mathbf{q}}, \tilde{\mathbf{q}}) \tilde{\mathbf{1}} = \mathbf{0}.$$

The first step is to contract (5.9), point-wise, with the entropy variables (at the continuous level this was the step $\mathcal{W} \frac{\partial \mathcal{F}_{x_m}}{\partial x_m} = \frac{\partial \mathcal{F}_{x_m}}{\partial x_m}$). This is accomplished by multiplying (5.9) by $\mathbf{1}_{\tilde{N}} \otimes \mathbf{1}_5^T \text{diag}(\mathbf{w}_\kappa)$, which results in

$$(5.10) \quad \mathcal{J} \mathbf{1}_{\tilde{N}} \otimes \mathbf{1}_5^T \text{diag}(\mathbf{w}_\kappa) \frac{d\tilde{\mathbf{q}}}{dt} + \mathbf{1}_{\tilde{N}} \otimes \mathbf{1}_5^T \text{diag}(\mathbf{w}_\kappa) \sum_{m=1}^3 \hat{D}_m \circ F_{x_m}(\tilde{\mathbf{q}}, \tilde{\mathbf{q}}) \tilde{\mathbf{1}} = \mathbf{0},$$

where \tilde{N} is the total number of nodes in the macro element. Adding and subtracting terms to (5.10) gives

$$(5.11) \quad \mathcal{J} \frac{d\tilde{\mathbf{s}}}{dt} + \mathbf{1}_{\tilde{N}} \otimes \mathbf{1}_5^T \sum_{m=1}^3 \left\{ \frac{1}{2} \text{diag}(\mathbf{w}_\kappa) \hat{D}_m \circ F_{x_m}(\tilde{\mathbf{q}}, \tilde{\mathbf{q}}) \tilde{\mathbf{1}} + \frac{1}{2} \hat{D}_m \text{diag}(\mathbf{w}_\kappa) \circ F_{x_m}(\tilde{\mathbf{q}}, \tilde{\mathbf{q}}) \tilde{\mathbf{1}} \right. \\ \left. + \frac{1}{2} \text{diag}(\mathbf{w}_\kappa) \hat{D}_m \circ F_{x_m}(\tilde{\mathbf{q}}, \tilde{\mathbf{q}}) \tilde{\mathbf{1}} - \frac{1}{2} \hat{D}_m \text{diag}(\mathbf{w}_\kappa) \circ F_{x_m}(\tilde{\mathbf{q}}, \tilde{\mathbf{q}}) \tilde{\mathbf{1}} \right\} = \mathbf{0}.$$

Consider the i^{th} term of the spatial terms of (5.11) (denoted $\text{Vol}(i)$ where $i = 1, \dots, \tilde{N}$),

$$(5.12) \quad \text{Vol}(i) \equiv \sum_{j=1}^{\tilde{N}} \bar{D}_m(i, j) \left\{ \frac{(\tilde{w}^{(i)} + \tilde{w}^{(j)})}{2} f_{x_m}^{\text{sc}}(\tilde{\mathbf{q}}^{(i)}, \tilde{\mathbf{q}}^{(j)}) + \frac{(\tilde{w}^{(i)} - \tilde{w}^{(j)})}{2} f_{x_m}^{\text{sc}}(\tilde{\mathbf{q}}^{(i)}, \tilde{\mathbf{q}}^{(j)}) \right\},$$

where $\hat{D}_m = \bar{D}_m \otimes \mathbf{I}_5$. Using the Tadmor shuffle condition (5.8) on the second set of terms results in

$$(5.13) \quad \text{Vol}(i) = \sum_{j=1}^{\tilde{N}} \bar{D}_m(i, j) \left\{ \frac{(\tilde{w}^{(i)} + \tilde{w}^{(j)})}{2} f_{x_m}^{\text{sc}}(\tilde{\mathbf{q}}^{(i)}, \tilde{\mathbf{q}}^{(j)}) + \frac{(\tilde{\psi}_{x_m}^{(i)} - \tilde{\psi}_{x_m}^{(j)})}{2} \right\}.$$

Adding and subtracting terms to (5.13) gives

$$(5.14) \quad \text{Vol}(i) = \sum_{j=1}^{\tilde{N}} \bar{D}_m(i, j) \left\{ \frac{(\tilde{w}^{(i)} + \tilde{w}^{(j)})}{2} f_{x_m}^{\text{sc}}(\tilde{\mathbf{q}}^{(i)}, \tilde{\mathbf{q}}^{(j)}) - \frac{(\tilde{\psi}_{x_m}^{(i)} + \tilde{\psi}_{x_m}^{(j)})}{2} \right\} \\ + \sum_{j=1}^{\tilde{N}} \bar{D}_m(i, j) \tilde{\psi}_{x_m}^{(i)}.$$

The last set of terms can be expanded into matrix form as (i.e., the vector constructed

from $\text{Vol}(\mathbf{i})$ for $i = 1, \dots, \tilde{N}$)

$$(5.15) \quad \left(\tilde{\psi}_{x_m} \right)^T \sum_{l=1}^3 \left\{ \bar{D}_{\xi_l} \left[\mathcal{J} \frac{\partial \xi_l}{\partial x_m} \right] + \left[\mathcal{J} \frac{\partial \xi_l}{\partial x_m} \right] \bar{D}_{\xi_l} \right\} \bar{\mathbf{1}} = \mathbf{0},$$

where the equality follows from the assumption that the discrete GCL conditions and consistency of the first derivative operator, i.e., $\bar{D}_{\xi_l} \bar{\mathbf{1}} = \mathbf{0}$. Eq. (5.14) can now be recast in terms of a new flux function matrix, $\tilde{F}_{x_m}(\tilde{\mathbf{q}}, \tilde{\mathbf{q}})$ constructed from the two-point flux function

$$\tilde{f}_{x_m}^{sc}(\tilde{\mathbf{q}}^{(i)}, \tilde{\mathbf{q}}^{(j)}) \equiv \frac{(\tilde{\mathbf{w}}^{(i)} + \tilde{\mathbf{w}}^{(j)})}{2} \mathbf{f}_{x_m}^{sc}(\tilde{\mathbf{q}}^{(i)}, \tilde{\mathbf{q}}^{(j)}) - \frac{(\tilde{\psi}_{x_m}^{(i)} + \tilde{\psi}_{x_m}^{(j)})}{2}.$$

Note that $\tilde{f}_{x_m}^{sc}$ is symmetric and consistent with \mathcal{F}_{x_m} ; thus, (5.10) reduces to

$$(5.16) \quad \mathbf{J} \frac{d\tilde{\mathbf{s}}}{dt} + \sum_{m=1}^3 \bar{D}_m \circ \tilde{F}_{x_m}(\tilde{\mathbf{q}}, \tilde{\mathbf{q}}) \bar{\mathbf{1}} = \mathbf{0},$$

where (see Appendix A in [15] for details on the approximation properties of the nonlinear operators)

$$\bar{D}_m \circ \tilde{F}_{x_m}(\tilde{\mathbf{q}}, \tilde{\mathbf{q}}) \bar{\mathbf{1}} \approx \frac{1}{2} \sum_{l=1}^3 \left\{ \frac{\partial}{\partial \xi_l} \left(\mathcal{J}_\kappa \frac{\partial \xi_l}{\partial x_m} \mathcal{F}_{x_m} \right) + \mathcal{J}_\kappa \frac{\partial \xi_l}{\partial x_m} \frac{\partial \mathcal{F}_{x_m}}{\partial \xi_l} \right\} (\tilde{\xi}).$$

Next, (5.16) is discretely integrated over the domain by left multiplying by $\bar{\mathbf{1}}^T \bar{\mathbf{P}}$ and rearranging, results in

$$(5.17) \quad \begin{aligned} \bar{\mathbf{1}}^T \bar{\mathbf{P}} \mathbf{J} \frac{d\tilde{\mathbf{s}}}{dt} &= - \sum_{m=1}^3 \bar{\mathbf{1}}^T \bar{\mathbf{Q}}_m \circ \tilde{F}_{x_m}(\tilde{\mathbf{q}}, \tilde{\mathbf{q}}) \bar{\mathbf{1}}, \\ &= - \frac{1}{2} \sum_{m=1}^3 \left\{ \bar{\mathbf{1}}^T \bar{\mathbf{Q}}_m \circ \tilde{F}_{x_m}(\tilde{\mathbf{q}}, \tilde{\mathbf{q}}) \bar{\mathbf{1}} + \bar{\mathbf{1}}^T \bar{\mathbf{Q}}_m^T \circ \tilde{F}_{x_m}(\tilde{\mathbf{q}}, \tilde{\mathbf{q}}) \bar{\mathbf{1}} \right\} \\ &= - \frac{1}{2} \sum_{m=1}^3 \left\{ \bar{\mathbf{1}}^T \bar{\mathbf{Q}}_m \circ \tilde{F}_{x_m}(\tilde{\mathbf{q}}, \tilde{\mathbf{q}}) \bar{\mathbf{1}} - \bar{\mathbf{1}}^T \bar{\mathbf{Q}}_m \circ \tilde{F}_{x_m}(\tilde{\mathbf{q}}, \tilde{\mathbf{q}}) \bar{\mathbf{1}} + \bar{\mathbf{1}}^T \bar{\mathbf{E}}_m \circ \tilde{F}_{x_m}(\tilde{\mathbf{q}}, \tilde{\mathbf{q}}) \bar{\mathbf{1}} \right\} \\ &= - \frac{1}{2} \sum_{m=1}^3 \bar{\mathbf{1}}^T \bar{\mathbf{E}}_m \circ \tilde{F}_{x_m}(\tilde{\mathbf{q}}, \tilde{\mathbf{q}}) \bar{\mathbf{1}} \\ &= - \frac{1}{2} \sum_{m=1}^3 \sum_{i,j=1}^N \bar{\mathbf{E}}_m(i,j) \left\{ \frac{(\tilde{\mathbf{w}}^{(i)} + \tilde{\mathbf{w}}^{(j)})}{2} \mathbf{f}_{x_m}^{sc}(\tilde{\mathbf{q}}^{(i)}, \tilde{\mathbf{q}}^{(j)}) - \frac{(\tilde{\psi}_{x_m}^{(i)} + \tilde{\psi}_{x_m}^{(j)})}{2} \right\} \\ &= - \frac{1}{2} \sum_{m=1}^3 \tilde{\mathbf{w}}^T \hat{\mathbf{E}}_m \circ \tilde{F}_{x_m}(\tilde{\mathbf{q}}, \tilde{\mathbf{q}}) \tilde{\mathbf{1}} + \frac{1}{2} \bar{\mathbf{1}}^T \bar{\mathbf{E}}_m \tilde{\psi}_m. \end{aligned}$$

Thus,

$$(5.18) \quad \bar{\mathbf{1}}^T \bar{\mathbf{P}} \mathbf{J} \frac{d\tilde{\mathbf{s}}}{dt} = - \frac{1}{2} \sum_{m=1}^3 \tilde{\mathbf{w}}^T \hat{\mathbf{E}}_m \circ \tilde{F}_{x_m}(\tilde{\mathbf{q}}, \tilde{\mathbf{q}}) \tilde{\mathbf{1}} + \frac{1}{2} \bar{\mathbf{1}}^T \bar{\mathbf{E}}_m \tilde{\psi}_m.$$

The right-hand side of (5.18) contains terms constructed from the \mathbf{E} matrices. As a result, these terms can be decomposed into the contributions of the separate surfaces of the element (node-wise). For periodic problems, these terms would cancel out with

the contributions from face SATs coupling terms leading to entropy conservation. For non-periodic problems appropriate SATs need to be constructed so that an entropy inequality or equality is attained (this is an active area of research; see, for example, [35, 43, 13]). It is important to highlight that when nonlinear systems of PDEs are considered, it is not possible to attain the telescoping property (5.11) by simply using SBP operators to discretely differentiate fluxes.

This section is finished by presenting the discretization for each element separately. The semi-discrete forms of the elements L and R are, respectively

(5.19)

$$\begin{aligned}
& \mathbf{J}_L \frac{d\mathbf{q}_L}{dt} + \sum_{l,m=1}^3 \left(\mathbf{D}_{\xi_l}^L \left[\mathcal{J} \frac{\partial \xi_l}{\partial x_m} \right]_L + \left[\mathcal{J} \frac{\partial \xi_m}{\partial x_l} \right]_L \mathbf{D}_{\xi_l}^L \right) \circ \mathbf{F}_{x_m}(\mathbf{q}_L, \mathbf{q}_L) \mathbf{1}_L = \\
& (\mathbf{P}^L)^{-1} \sum_{m=1}^3 \left\{ \left(\mathbf{e}_{N_L} \mathbf{e}_{N_L}^T \mathbf{P}_L^{(1D)} \otimes \mathbf{P}_L^{(1D)} \otimes \mathbf{I}_5 \right) \left[\mathcal{J} \frac{\partial \xi_1}{\partial x_m} \right]_L \right\} \circ \mathbf{F}_{x_m}(\mathbf{q}_L, \mathbf{q}_L) \mathbf{1}_L \\
& (\mathbf{P}^L)^{-1} \sum_{m=1}^3 \left\{ \left[\mathcal{J} \frac{\partial \xi_1}{\partial x_m} \right]_L \left(\mathbf{e}_{N_L} \mathbf{e}_{N_L}^T \mathbf{P}_L^{(1D)} \otimes \mathbf{P}_L^{(1D)} \otimes \mathbf{I}_5 \right) \right\} \circ \mathbf{F}_{x_m}(\mathbf{q}_L, \mathbf{q}_L) \mathbf{1}_L \\
& - (\mathbf{P}^L)^{-1} \sum_{m=1}^3 \left\{ \left(\mathbf{e}_{N_L} \otimes \mathbf{I}_{N_L} \otimes \mathbf{I}_{N_L} \otimes \mathbf{I}_5 \right) \left[\mathcal{J} \frac{\partial \xi_1}{\partial x_m} \right]_L^{\hat{\Gamma}} \left(\mathbf{P}_L^{(1D)} \mathbf{I}_{\text{HtoL}}^{(1D)} \otimes \mathbf{P}_L^{(1D)} \mathbf{I}_{\text{HtoL}}^{(1D)} \otimes \mathbf{I}_5 \right) \right. \\
& \left. \left(\mathbf{e}_{\text{I}_H}^T \otimes \mathbf{I}_{N_H} \otimes \mathbf{I}_{N_H} \otimes \mathbf{I}_5 \right) \right\} \circ \mathbf{F}_{x_m}(\mathbf{q}_L, \mathbf{q}_H) \mathbf{1}_H \\
& - (\mathbf{P}^L)^{-1} \sum_{m=1}^3 \left\{ \left(\mathbf{e}_{N_L} \otimes \mathbf{I}_{N_L} \otimes \mathbf{I}_{N_L} \otimes \mathbf{I}_5 \right) \left(\mathbf{P}_L^{(1D)} \mathbf{I}_{\text{HtoL}}^{(1D)} \otimes \mathbf{P}_L^{(1D)} \mathbf{I}_{\text{HtoL}}^{(1D)} \otimes \mathbf{I}_5 \right) \left[\mathcal{J} \frac{\partial \xi_1}{\partial x_m} \right]_H^{\hat{\Gamma}} \right. \\
& \left. \left(\mathbf{e}_{\text{I}_H}^T \otimes \mathbf{I}_{N_H} \otimes \mathbf{I}_{N_H} \otimes \mathbf{I}_5 \right) \right\} \circ \mathbf{F}_{x_m}(\mathbf{q}_L, \mathbf{q}_H) \mathbf{1}_H, \\
& \text{and}
\end{aligned}$$

(5.20)

$$\begin{aligned}
& \mathbf{J}_H \frac{d\mathbf{q}_H}{dt} + \sum_{l,m=1}^3 \left(\mathbf{D}_{\xi_l}^H \left[\mathcal{J} \frac{\partial \xi_l}{\partial x_m} \right]_H + \left[\mathcal{J} \frac{\partial \xi_m}{\partial x_l} \right]_H \mathbf{D}_{\xi_l}^H \right) \circ \mathbf{F}_{x_m}(\mathbf{q}_H, \mathbf{q}_H) \mathbf{1}_L = \\
& - (\mathbf{P}^H)^{-1} \sum_{m=1}^3 \left\{ \left(\mathbf{e}_{\text{I}_H} \mathbf{e}_{\text{I}_H}^T \mathbf{P}_H^{(1D)} \otimes \mathbf{P}_H^{(1D)} \otimes \mathbf{I}_5 \right) \left[\mathcal{J} \frac{\partial \xi_1}{\partial x_m} \right]_H \right\} \circ \mathbf{F}_{x_m}(\mathbf{q}_H, \mathbf{q}_H) \mathbf{1}_H \\
& - (\mathbf{P}^H)^{-1} \sum_{m=1}^3 \left\{ \left[\mathcal{J} \frac{\partial \xi_1}{\partial x_m} \right]_H \left(\mathbf{e}_{\text{I}_H} \mathbf{e}_{\text{I}_H}^T \mathbf{P}_H^{(1D)} \otimes \mathbf{P}_H^{(1D)} \otimes \mathbf{I}_5 \right) \right\} \circ \mathbf{F}_{x_m}(\mathbf{q}_H, \mathbf{q}_H) \mathbf{1}_H \\
& + (\mathbf{P}^H)^{-1} \sum_{m=1}^3 \left\{ \left(\mathbf{e}_{\text{I}_H} \otimes \mathbf{I}_{N_H} \otimes \mathbf{I}_{N_H} \otimes \mathbf{I}_5 \right) \left[\mathcal{J} \frac{\partial \xi_1}{\partial x_m} \right]_H^{\hat{\Gamma}} \left(\mathbf{P}_H^{(1D)} \mathbf{I}_{\text{LtoH}}^{(1D)} \otimes \mathbf{P}_H^{(1D)} \mathbf{I}_{\text{LtoH}}^{(1D)} \otimes \mathbf{I}_5 \right) \right. \\
& \left. \left(\mathbf{e}_{N_L}^T \otimes \mathbf{I}_{N_L} \otimes \mathbf{I}_{N_L} \otimes \mathbf{I}_5 \right) \right\} \circ \mathbf{F}_{x_m}(\mathbf{q}_H, \mathbf{q}_L) \mathbf{1}_L \\
& + (\mathbf{P}^H)^{-1} \sum_{m=1}^3 \left\{ \left(\mathbf{e}_{\text{I}_H} \otimes \mathbf{I}_{N_H} \otimes \mathbf{I}_{N_H} \otimes \mathbf{I}_5 \right) \left(\mathbf{P}_H^{(1D)} \mathbf{I}_{\text{LtoH}}^{(1D)} \otimes \mathbf{P}_H^{(1D)} \mathbf{I}_{\text{LtoH}}^{(1D)} \otimes \mathbf{I}_5 \right) \left[\mathcal{J} \frac{\partial \xi_1}{\partial x_m} \right]_L^{\hat{\Gamma}} \right. \\
& \left. \left(\mathbf{e}_{N_L}^T \otimes \mathbf{I}_{N_L} \otimes \mathbf{I}_{N_L} \otimes \mathbf{I}_5 \right) \right\} \circ \mathbf{F}_{x_m}(\mathbf{q}_H, \mathbf{q}_L) \mathbf{1}_L.
\end{aligned}$$

The algorithm presented above leads to an entropy conservative discretization (modulo what boundary conditions are imposed). However, the main interest is in

entropy stable algorithms and the approach use herein to achieve this is to augment the entropy conservative scheme with an appropriate interface dissipation. How this is accomplished is discussed in the next section.

6 Inviscid interface dissipation and boundary SATs To make the inviscid entropy conservative scheme entropy stable, an interface dissipation needs to be added. Herein, as in the conforming algorithms [3, 35, 7, 33], the numerical dissipation is motivated by the up-winding used in a Roe approximate Riemann solver which has the form

$$(6.1) \quad \mathcal{F}^* = \frac{\mathcal{F}^+ + \mathcal{F}^-}{2} - \frac{1}{2} \Upsilon |\Lambda| \Upsilon^{-1} (\mathcal{Q}^+ - \mathcal{Q}^-),$$

where $+$ and $-$ refer to quantities evaluated on the side of the interface in the positive and negative face normal directions, respectively (see Figure 1).

The original Roe flux: \mathcal{F}^* is composed of an inviscid flux average: $(\mathcal{F}^+ + \mathcal{F}^-)/2$ and a dissipation term. The flux average term is not in general entropy conservative, and is replaced with an entropy conservative two-point flux, e.g., Chandrashekar [9] or Ismail and Roe [27]. The remaining dissipation term, is reformulated in quadratic form to facilitate an entropy stability proof. This step is accomplished by using the flux Jacobian with respect to the entropy variables, \mathcal{W} , rather than the conservative variables, \mathcal{Q} . A unique scaling of the eigenvectors of the conservative variable flux Jacobian facilitates the reformulation [30].

$$\frac{\partial \mathcal{Q}}{\partial \mathcal{W}} = \Upsilon \Upsilon^T \quad ; \quad \frac{\partial \mathcal{F}_{\xi_i}}{\partial \mathcal{W}} = \frac{\partial \mathcal{F}_{\xi_i}}{\partial \mathcal{Q}} \frac{\partial \mathcal{Q}}{\partial \mathcal{W}} = \Upsilon \Lambda_{\xi_i} \Upsilon^{-1} \Upsilon \Upsilon^T = \Upsilon \Lambda_{\xi_i} \Upsilon^T$$

A full description of the various required matrices appears in Fisher [19].

The interface dissipation term: $\Upsilon |\Lambda| \Upsilon^{-1} (\mathcal{Q}^+ - \mathcal{Q}^-)$ is replaced with the equivalent quadratic dissipation term: $\Upsilon |\Lambda| \Upsilon^T (\mathcal{W}^+ - \mathcal{W}^-)$. The final form of the interface flux is

$$(6.2) \quad \mathcal{F}^* = \mathbf{f}_{x_m}^{sc}(\mathcal{W}^+, \mathcal{W}^-) - \frac{1}{2} \Upsilon |\Lambda| \Upsilon^T (\mathcal{W}^+ - \mathcal{W}^-).$$

and leads to an entropy stable scheme. The extension to the curvilinear case follows immediately by constructing all three computational fluxes followed by the dot product with the outward facing normal.

Therefore, the dissipation on element L is given as

$$(6.3) \quad \begin{aligned} \mathit{diss}_L \equiv & -\frac{1}{2} (\mathbf{P}^L)^{-1} \mathbf{R}_L^T \mathbf{P}_{\perp \xi_1}^L \left| \frac{\partial \mathcal{F}_{\xi_1}}{\partial \mathcal{W}} \right|_L (\mathbf{R}_L \mathbf{w}_L - \mathbf{l}_{\text{HtoL}} \mathbf{R}_H \mathbf{w}_H) \\ & - \frac{1}{2} (\mathbf{P}^L)^{-1} \mathbf{R}_L^T \mathbf{P}_{\perp \xi_1}^L \mathbf{l}_{\text{HtoL}} \left| \frac{\partial \mathcal{F}_{\xi_1}}{\partial \mathcal{W}} \right|_H (\mathbf{l}_{\text{LtoH}} \mathbf{R}_L \mathbf{w}_L - \mathbf{R}_H \mathbf{w}_H), \end{aligned}$$

and on element H takes the following form

$$(6.4) \quad \begin{aligned} \mathit{diss}_H \equiv & -\frac{1}{2} (\mathbf{P}^H)^{-1} \mathbf{R}_H^T \mathbf{P}_{\perp \xi_1}^H \left| \frac{\partial \mathcal{F}_{\xi_1}}{\partial \mathcal{W}} \right|_H (\mathbf{R}_H \mathbf{w}_H - \mathbf{l}_{\text{LtoH}} \mathbf{R}_L \mathbf{w}_L) \\ & - \frac{1}{2} (\mathbf{P}^H)^{-1} \mathbf{R}_H^T \mathbf{P}_{\perp \xi_1}^H \mathbf{l}_{\text{LtoH}} \left| \frac{\partial \mathcal{F}_{\xi_1}}{\partial \mathcal{W}} \right|_L (\mathbf{l}_{\text{HtoL}} \mathbf{R}_H \mathbf{w}_H - \mathbf{R}_L \mathbf{w}_L), \end{aligned}$$

where $\left| \frac{\partial \mathcal{F}_{\xi_1}}{\partial \mathcal{W}} \right|_L$ is constructed from the Roe average of the states \mathbf{w}_L and $\mathbf{l}_{\text{HtoL}} \mathbf{w}_H$, and $\left| \frac{\partial \mathcal{F}_{\xi_1}}{\partial \mathcal{W}} \right|_H$ is constructed from the Roe average of the states \mathbf{w}_H and $\mathbf{l}_{\text{LtoH}} \mathbf{w}_L$. Furthermore, the various operators which appear in (6.3) and (6.4) are defined as

follows:

$$\begin{aligned} \mathbf{R}_L &\equiv \mathbf{e}_{N_L}^T \otimes \mathbf{I}_{N_L} \otimes \mathbf{I}_{N_L} \otimes \mathbf{I}_5, & \mathbf{R}_H &\equiv \mathbf{e}_{I_H}^T \otimes \mathbf{I}_{N_H} \otimes \mathbf{I}_{N_H} \otimes \mathbf{I}_5, \\ \mathbf{P}_{\perp \xi_i}^L &\equiv \mathbf{P}_L^{(1D)} \otimes \mathbf{P}_L^{(1D)} \otimes \mathbf{I}_5, & \mathbf{P}_{\perp \xi_i}^H &\equiv \mathbf{P}_H^{(1D)} \otimes \mathbf{P}_H^{(1D)} \otimes \mathbf{I}_5, \\ \mathbf{I}_{HtoL} &\equiv \mathbf{I}_{HtoL}^{(1D)} \otimes \mathbf{I}_{HtoL}^{(1D)} \otimes \mathbf{I}_5, & \mathbf{I}_{LtoH} &\equiv \mathbf{I}_{LtoH}^{(1D)} \otimes \mathbf{I}_{LtoH}^{(1D)} \otimes \mathbf{I}_5. \end{aligned}$$

HERE1234 All the theorems regarding the accuracy and the entropy stability are presented (element-wise conservation is discussed in Appendix E in [15] while it is straightforward to see that free-stream preservation is attained if the discrete GCL are satisfied).

THEOREM 4. *The dissipation term \mathbf{diss}_L is a term of order $p_L + d - 1$ and the dissipation term \mathbf{diss}_H is a term of order $p_L + d - 1$.*

Proof. This follows from the accuracy of the interpolation operators. \square

THEOREM 5. *The dissipation terms (6.3) and (6.4) lead to an entropy stable scheme.*

Proof. Contracting the global dissipation operator with the entropy variables results in contractions of the interface dissipation terms \mathbf{diss}_L and \mathbf{diss}_H by $\mathbf{w}_L^T \mathbf{P}^L$ and $\mathbf{w}_H^T \mathbf{P}^H$, respectively. Summing the interface contributions $\mathbf{w}_L^T \mathbf{P}^L \mathbf{diss}_L$ and $\mathbf{w}_H^T \mathbf{P}^H \mathbf{diss}_H$, using the property $\mathbf{I}_{HtoL} = (\mathbf{P}^L)^{-1} \mathbf{I}_{LtoH}^T \mathbf{P}^H$ and rearranging terms, results in

$$\begin{aligned} &\mathbf{w}_L^T \mathbf{P}^L \mathbf{diss}_L + \mathbf{w}_H^T \mathbf{P}^H \mathbf{diss}_H = \\ &-\frac{1}{2} (\mathbf{R}_L \mathbf{w}_L - \mathbf{I}_{HtoL} \mathbf{R}_H \mathbf{w}_H)^T \mathbf{P}_{\perp \xi_1}^L \left| \frac{\partial \mathcal{F}_{\xi_1}}{\partial \mathcal{W}} \right|_L (\mathbf{R}_L \mathbf{w}_{rmL} - \mathbf{I}_{HtoL} \mathbf{R}_H \mathbf{w}_{rmH}) \\ &-\frac{1}{2} (\mathbf{R}_H \mathbf{w}_{rmH} - \mathbf{I}_{LtoH} \mathbf{R}_L \mathbf{w}_L)^T \mathbf{P}_{\perp \xi_1}^H \left| \frac{\partial \mathcal{F}_{\xi_1}}{\partial \mathcal{W}} \right|_H (\mathbf{R}_H \mathbf{w}_H - \mathbf{I}_{LtoH} \mathbf{R}_L \mathbf{w}_L), \end{aligned}$$

which is a negative semi-definite term. Therefore, the added interface terms are entropy dissipative. \square

In Section 7, two problems are used to characterize the nonconforming algorithms: 1) the propagation of an isentropic vortex and 2) the inviscid Taylor-Green vortex problem. For all of them, the boundary conditions are weakly imposed by reusing the interface SAT mechanics (see, for instance, [35, 13]).

7 Numerical experiments This section presents numerical evidence that demonstrates that the proposed p nonconforming algorithm retains the accuracy and robustness of the spatial conforming discretization reported in [3, 35, 7, 33].

Herein, the conforming [3, 35, 7, 33] and p -adaptive solver for unstructured grids developed at the Extreme Computing Research Center (ECRC) at KAUST is used to perform numerical experiments. This parallel solver is built on top of the Portable and Extensible Toolkit for Scientific computing (PETSc) [2], its mesh topology abstraction (DMPLEX) [28] and scalable ordinary differential equation (ODE)/differential algebraic equations (DAE) solver library [1]. The systems of ordinary differential equations arising from the spatial discretizations are integrated using the fourth-order accurate Dormand–Prince method [18] endowed with an adaptive time stepping technique based on digital signal processing [40, 41]. To make the temporal error negligible, a tolerance of 10^{-8} is always used for the time-step adaptivity. The two-point entropy consistent flux of Chandrashekar [9] is used for all the test cases.

The errors are computed using volume scaled (for the L^1 and L^2 norms) discrete

norms as follows:

$$\begin{aligned} \|\mathbf{u}\|_{L^1} &= \Omega_c^{-1} \sum_{\kappa=1}^K \mathbf{1}_\kappa^T \mathbf{P}^\kappa \mathbf{J}_\kappa \text{abs}(\mathbf{u}_\kappa), \quad \|\mathbf{u}\|_{L^2}^2 = \Omega_c^{-1} \sum_{\kappa=1}^K \mathbf{u}_\kappa^T \mathbf{P}^\kappa \mathbf{J}_\kappa \mathbf{u}_\kappa, \\ \|\mathbf{u}\|_{L^\infty} &= \max_{\kappa=1 \dots K} \text{abs}(\mathbf{u}_\kappa), \end{aligned}$$

where Ω_c indicates the volume of Ω computed as $\Omega_c \equiv \sum_{\kappa=1}^K \mathbf{1}_\kappa^T \mathbf{P}^\kappa \mathbf{J}_\kappa \mathbf{1}_\kappa$.

7.1 Isentropic Euler vortex propagation For verification and characterization of the inviscid components of the algorithm, the propagation of an isentropic vortex is used. This benchmark problem has an analytical solution which is given by

$$\begin{aligned} \mathcal{G}(x_1, x_2, x_3, t) &= 1 - \left\{ [(x_1 - x_{1,0}) - U_\infty \cos(\alpha) t]^2 + [(x_2 - x_{2,0}) - U_\infty \sin(\alpha) t]^2 \right\}, \\ \rho &= T^{\frac{1}{\gamma-1}}, \\ \mathcal{U}_1 &= U_\infty \cos(\alpha) - \epsilon_\nu \frac{(x_2 - x_{2,0}) - U_\infty \sin(\alpha) t}{2\pi} \exp\left(\frac{\mathcal{G}}{2}\right), \\ \mathcal{U}_2 &= U_\infty \sin(\alpha) - \epsilon_\nu \frac{(x_1 - x_{1,0}) - U_\infty \cos(\alpha) t}{2\pi} \exp\left(\frac{\mathcal{G}}{2}\right), \\ \mathcal{U}_3 &= 0, \\ T &= \left[1 - \epsilon_\nu^2 M_\infty^2 \frac{\gamma-1}{8\pi^2} \exp(\mathcal{G}) \right], \end{aligned}$$

where U_∞ , M_∞ , and $(x_{1,0}, x_{2,0}, x_{3,0})$ are the modulus of the freestream velocity, the freestream Mach number, and the vortex center, respectively. In this paper, the following values are used: $U_\infty = M_\infty c_\infty$, $\epsilon_\nu = 5$, $M_\infty = 0.5$, $\gamma = 1.4$, $\alpha = 45^\circ$, and $(x_{1,0}, x_{2,0}, x_{3,0}) = (0, 0, 0)$. The computational domain is $x_1 \in [-5, 5]$, $x_2 \in [-5, 5]$, $x_3 \in [-5, 5]$, and $t \in [0, 2]$. The analytical solution is used to furnish data for the initial condition.

First, results aimed at validating the entropy conservation properties of the interior domain SBP-SAT algorithm are reported. Thus, periodic boundary conditions are used on all six faces of the computational domain. Furthermore, all the dissipation terms used for the interface coupling are turned off. The discrete integral over the computational domain of the time rate of change of the entropy function, $\int_\Omega \frac{\partial \mathcal{S}}{\partial t} d\Omega$ in Eq. (5.5), is monitored at every time step.

The computational domain is subdivided using ten hexahedrons in each coordinate direction and the solution polynomial degree in each element is assigned a random integer chosen uniformly from the set $p_s = \{2, 3, 4, 5\}$ (i.e., each member in the set has an equal probability of being chosen). To test the conservation of entropy and therefore the freestream condition when curved element interfaces are used, the LGL collocation point coordinates at element interfaces are constructed¹ as follows:

- Construct a mesh by describing the element interfaces with a second-order polynomial representation. Note that many mesh generators use a uniform distribution of points (or nodes) to construct such a geometrical representation.
- Perturb the nodes that are used to define the second-order polynomial ap-

¹In a general setting, element interfaces can also be boundary element interfaces.

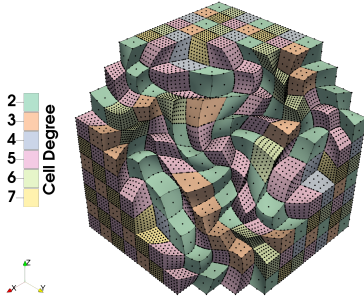


FIG. 2. *Isentropic vortex: mesh cut and polynomial order distribution.*

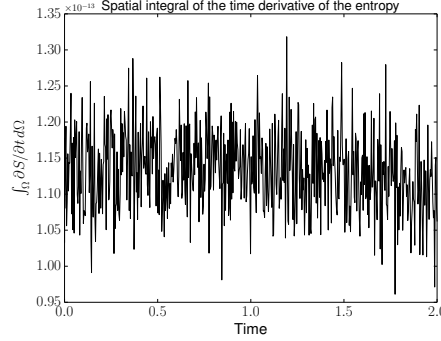


FIG. 3. *Isentropic vortex: time rate of change of the entropy function.*

proximation of the element interfaces as follows:

$$x_1 = x_{1,*} + \frac{1}{15}L_1 \cos(a) \cos(3b) \sin(4c), \quad x_2 = x_{2,*} + \frac{1}{15}L_2 \sin(4a) \cos(b) \cos(3c),$$

$$x_3 = x_{3,*} + \frac{1}{15}L_3 \cos(3a) \sin(4b) \cos(c),$$

where

$$a = \frac{\pi}{L_1} \left(x_{1,*} - \frac{x_{1,H} + x_{1,L}}{2} \right), \quad b = \frac{\pi}{L_2} \left(x_{2,*} - \frac{x_{2,H} + x_{2,L}}{2} \right),$$

$$c = \frac{\pi}{L_3} \left(x_{3,*} - \frac{x_{3,H} + x_{3,L}}{2} \right).$$

The lengths L_1 , L_2 and L_3 are the dimensions of the computational domain in the three coordinate directions and the sub-script * indicates the unperturbed coordinates of the nodes. This step yields a “perturbed” second-order interface polynomial representation.

- Compute the coordinate of the LGL points at the element interface by evaluating the “perturbed” second-order polynomial at the tensor-product LGL points used to define the cell solution polynomial of order p_s .

Figure 2 shows a cut of the mesh and the polynomial order distribution used for this first test case. The propagation of the vortex is simulated for two time units. Figure 3 plots the integral of the time derivative of the entropy function. It is seen that the global variation of the time rate of the of \mathcal{S} is practically zero. This implies that the spatially nonconforming algorithm is entropy conservative.

Second, a grid convergence study is performed to investigate the order of convergence of the nonconforming algorithm. The base grid (i.e., the coarsest grid) is constructed as follows:

- Divide the computational domain with four hexahedral elements in each coordinate direction.
- Assign the solution polynomial degree in each element to a random integer chosen uniformly from the set $\{p_s, p_s + 1\}$.
- Approximate with a p_s -th-order accurate polynomial the element interfaces.
- Construct the perturbed elements and their corresponding LGL points as described previously.

From the base grid, which is similar to the one depicted in Figure 2, a sequence of

nested grids is then generated to perform the convergence study. The results are reported in Tables 1 through 6 for the error on the density. The number listed in the first column denoted by “Grid” indicates the number of hexahedrons in each coordinate direction.

Grid	Conforming, $p = 1$						Nonconforming, $p = 1$ and $p = 2$					
	L^1	Rate	L^2	Rate	L^∞	Rate	L^1	Rate	L^2	Rate	L^∞	Rate
4	2.74E-02	-	1.32E-03	-	1.55E-01	-	1.87E-02	-	9.48E-04	-	1.20E-01	-
8	1.14E-02	-1.26	6.61E-04	-1.00	1.12E-01	-0.47	1.02E-02	-0.87	5.87E-04	-0.69	1.23E-01	+0.04
16	5.13E-03	-1.16	3.31E-04	-1.00	7.29E-02	-0.62	4.55E-03	-1.17	2.99E-04	-0.97	7.06E-02	-0.80
32	1.70E-03	-1.59	1.15E-04	-1.52	3.01E-02	-1.28	1.52E-03	-1.58	1.07E-04	-1.49	3.97E-02	-0.83
64	4.76E-04	-1.84	3.24E-05	-1.83	8.53E-03	-1.82	4.36E-04	-1.81	3.15E-05	-1.76	2.15E-02	-0.88
128	1.23E-04	-1.96	8.33E-06	-1.96	2.13E-03	-2.00	1.14E-04	-1.93	8.72E-06	-1.85	1.05E-02	-1.03
256	3.08E-05	-1.99	2.09E-06	-1.99	5.24E-04	-2.02	2.91E-05	-1.98	2.46E-06	-1.83	5.10E-03	-1.05
512	7.68E-06	-2.00	5.23E-07	-2.00	1.30E-04	-2.01	7.23E-06	-2.01	6.17E-07	-2.00	2.26E-03	-1.17

TABLE 1

Convergence study of the isentropic vortex propagation: $p = 1$ with $p = 2$; density error.

Grid	Conforming, $p = 2$						Nonconforming, $p = 2$ and $p = 3$					
	L^1	Rate	L^2	Rate	L^∞	Rate	L^1	Rate	L^2	Rate	L^∞	Rate
4	9.75E-03	-	5.32E-04	-	1.24E-01	-	8.57E-03	-	5.05E-04	-	1.21E-01	-
8	3.18E-03	-1.61	2.09E-04	-1.35	6.97E-02	-0.83	2.70E-03	-1.67	1.84E-04	-1.46	8.55E-02	-0.50
16	5.18E-04	-2.62	3.88E-05	-2.43	2.51E-02	-1.47	4.25E-04	-2.67	3.58E-05	-2.36	3.23E-02	-1.40
32	6.38E-05	-3.02	5.50E-06	-2.82	7.23E-03	-1.79	4.99E-05	-3.09	5.14E-06	-2.80	7.20E-03	-2.17
64	7.61E-06	-3.07	7.23E-07	-2.93	1.21E-03	-2.58	5.78E-06	-3.11	7.05E-07	-2.87	1.42E-03	-2.35
128	9.48E-07	-3.00	9.95E-08	-2.86	2.75E-04	-2.14	7.14E-07	-3.02	1.06E-07	-2.74	3.52E-04	-2.01
256	1.23E-07	-2.94	1.43E-08	-2.83	3.41E-05	-3.01	9.46E-08	-2.92	1.52E-08	-2.80	9.16E-05	-1.94

TABLE 2

Convergence study of the isentropic vortex propagation: $p = 2$ with $p = 3$; density error.

Grid	Conforming, $p = 3$						Nonconforming, $p = 3$ and $p = 4$					
	L^1	Rate	L^2	Rate	L^∞	Rate	L^1	Rate	L^2	Rate	L^∞	Rate
4	5.22E-03	-	3.38E-04	-	9.16E-02	-	4.58E-03	-	3.07E-04	-	8.90E-02	-
8	6.84E-04	-2.93	5.30E-05	-2.67	4.71E-02	-0.96	5.81E-04	-2.98	4.94E-05	-2.63	5.26E-02	-0.76
16	5.50E-05	-3.64	4.54E-06	-3.55	6.61E-03	-2.83	4.51E-05	-3.69	4.15E-06	-3.58	5.04E-03	-3.38
32	3.48E-06	-3.98	3.33E-07	-3.77	5.47E-04	-3.59	2.88E-06	-3.97	3.06E-07	-3.76	4.98E-04	-3.34
64	2.10E-07	-4.05	2.45E-08	-3.76	4.93E-05	-3.47	1.78E-07	-4.01	2.34E-08	-3.71	5.42E-05	-3.20
128	1.39E-08	-3.92	1.87E-09	-3.71	6.32E-06	-2.96	1.24E-08	-3.85	1.90E-09	-3.63	7.96E-06	-2.77

TABLE 3

Convergence study of the isentropic vortex propagation: $p = 3$ with $p = 4$; density error.

For all the degrees tested (i.e., $p = 1$ to $p = 7$), the order of convergence of the conforming algorithm is very close to that of the nonconforming. However, note that in the L^1 and L^2 norms the nonconforming algorithm is more accurate than the conforming one. In the discrete L^∞ norm, the nonconforming scheme is sometimes slightly worse than the conforming scheme; this results from the interpolation matrices being sub-optimal at nonconforming interfaces.

Grid	Conforming, $p = 4$						Nonconforming, $p = 4$ and $p = 5$					
	L^1	Rate	L^2	Rate	L^∞	Rate	L^1	Rate	L^2	Rate	L^∞	Rate
4	2.34E-03	-	1.56E-04	-	9.92E-02	-	2.10E-03	-	1.48E-04	-	9.28E-02	-
8	1.70E-04	-3.78	1.43E-05	-3.45	2.32E-02	-2.09	1.48E-04	-3.82	1.37E-05	-3.43	2.30E-02	-2.01
16	6.07E-06	-4.81	6.41E-07	-4.48	1.27E-03	-4.19	5.17E-06	-4.85	6.00E-07	-4.51	1.26E-03	-4.19
32	1.99E-07	-4.93	2.25E-08	-4.83	5.13E-05	-4.64	1.64E-07	-4.98	2.07E-08	-4.86	5.50E-05	-4.52
64	7.11E-09	-4.81	8.60E-10	-4.71	3.01E-06	-4.09	6.36E-09	-4.69	7.95E-10	-4.70	2.99E-06	-4.20

TABLE 4

Convergence study of the isentropic vortex propagation: $p = 4$ with $p = 5$; density error.

Grid	Conforming, $p = 5$						Nonconforming, $p = 5$ and $p = 6$					
	L^1	Rate	L^2	Rate	L^∞	Rate	L^1	Rate	L^2	Rate	L^∞	Rate
4	1.01E-03	-	6.88E-05	-	4.53E-02	-	9.14E-04	-	6.63E-05	-	4.45E-02	-
8	3.81E-05	-4.73	3.80E-06	-4.18	6.37E-03	-2.83	3.26E-05	-4.81	3.61E-06	-4.20	6.44E-03	-2.79
16	7.23E-07	-5.72	7.95E-08	-5.58	2.23E-04	-4.84	5.93E-07	-5.78	7.30E-08	-5.63	1.63E-04	-5.30
32	1.24E-08	-5.87	1.59E-09	-5.65	4.99E-06	-5.48	1.05E-08	-5.82	1.46E-09	-5.65	4.99E-06	-5.03

TABLE 5

Convergence study of the isentropic vortex propagation: $p = 5$ with $p = 6$; density error.

Grid	Conforming, $p = 6$						Nonconforming, $p = 6$ and $p = 7$					
	L^1	Rate	L^2	Rate	L^∞	Rate	L^1	Rate	L^2	Rate	L^∞	Rate
4	4.28E-04	-	3.14E-05	-	2.17E-02	-	3.84E-04	-	3.03E-05	-	2.35E-02	-
8	8.58E-06	-5.64	9.16E-07	-5.10	1.57E-03	-3.78	7.27E-06	-5.72	8.72E-07	-5.12	1.58E-03	-3.89
16	7.97E-08	-6.75	1.02E-08	-6.49	2.20E-05	-6.16	6.58E-08	-6.79	9.41E-09	-6.53	2.37E-05	-6.06
32	5.95E-10	-7.07	8.17E-11	-6.96	2.55E-07	-6.43	6.05E-10	-6.76	7.71E-11	-6.93	3.55E-07	-6.06

TABLE 6

Convergence study of the isentropic vortex propagation: $p = 6$ with $p = 7$; density error.

7.2 Inviscid Taylor–Green vortex propagation The purpose of this section is to demonstrate that robustness of the nonconforming entropy stable algorithm. To do so, the inviscid Taylor–Green vortex problem is solved using a coarse grid with four elements in each coordinate direction.

The test case is solved on a periodic cube $[-\pi L \leq x, y, z \leq \pi L]$, where the initial condition is given by the initial condition used for the simulation of the standard (viscous) Taylor–Green problem:

$$\mathcal{U}_1 = \mathcal{V}_0 \sin\left(\frac{x_1}{L}\right) \cos\left(\frac{x_2}{L}\right) \cos\left(\frac{x_3}{L}\right), \mathcal{U}_2 = -\mathcal{V}_0 \cos\left(\frac{x_1}{L}\right) \sin\left(\frac{x_2}{L}\right) \cos\left(\frac{x_3}{L}\right),$$

$$\mathcal{U}_3 = 0, \mathcal{P} = \mathcal{P}_0 + \frac{\rho_0 \mathcal{V}_0^2}{16} \left[\cos\left(\frac{2x_1}{L}\right) + \cos\left(\frac{2x_2}{L}\right) \right] \left[\cos\left(\frac{2x_3}{L}\right) + 2 \right].$$

The flow is initialized using $\mathcal{P}/\rho = \mathcal{P}_0/\rho_0 = R\mathcal{T}_0$, and $\mathcal{P}_0 = 1$, $\mathcal{T}_0 = 1$, $L = 1$, and $\mathcal{V}_0 = 1$. In order to obtain results that are reasonably close to those found for the incompressible equations, a Mach number of $M = 0.05$ is used.

The problem is simulated for twenty time units using an unstructured grid constructed as follows:

- Divide the computational domain with four hexahedral elements in each coordinate direction.

- Assign the solution polynomial degree in each element to a random integer chosen uniformly from a set $\{p_{min}, p_{max}\}$.
- Approximate the element interfaces with a p_{min} th accurate polynomial.
- Construct the perturbed elements and their corresponding LGL points as described in Section 7.1.

Figure 4 shows the time rate of change of the kinetic energy, dke/dt , for the nonconforming algorithm using a random distribution of solution polynomial order between i) $p_{min} = 2$ and $p_{max} = 7$ and ii) $p_{min} = 2$ and $p_{max} = 10$. The main take-

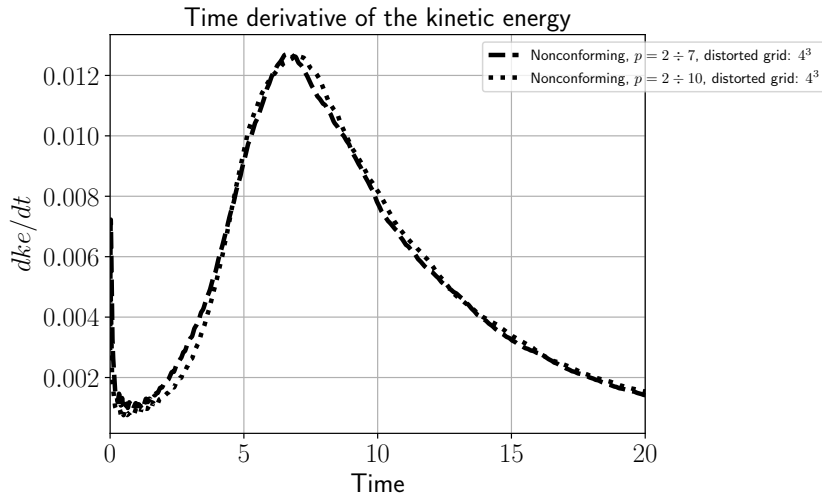


FIG. 4. Evolution of the time derivative of the kinetic energy for the inviscid Taylor–Green vortex at $M = 0.05$.

away from the figure is that all simulations are stable. This is numerical evidence that the p -nonconforming scheme inherits the stability characteristics of the conforming and fully staggered algorithms [3, 35, 4, 7, 33].

8 Conclusions In this paper, the entropy conservative p -refinement/coarsening nonconforming algorithm of Friedrich *et al.* [24] is extended to curvilinear coordinates applicable to the compressible Euler equations. The coupling between nonconforming interfaces is achieved using SBP preserving interpolation operators and prescribed metric terms. To maintain entropy conservation/stability, elementwise conservation, and the order of the parent element, the procedure of Crean *et al.* [11] is used to approximate grid metrics. Finally, the accuracy and stability characteristics of the resulting numerical schemes are shown to be comparable to those of the original conforming scheme [3, 35], in the context of two canonical tests.

Acknowledgments Special thanks are extended to Dr. Mujeeb R. Malik for partially funding this work as part of NASA’s “Transformational Tools and Technologies” (T^3) project. The research reported in this publication was also supported by funding from King Abdullah University of Science and Technology (KAUST). We are thankful for the computing resources of the Supercomputing Laboratory and the Extreme Computing Research Center at KAUST. Gregor Gassner and Lucas Friedrich has been supported by the European Research Council (ERC) under the European Unions Eight Framework Program Horizon 2020 with the research project Extreme, ERC grant agreement no. 714487.

REFERENCES

- [1] S. ABHYANKAR, J. BROWN, E. M. CONSTANTINESCU, D. GHOSH, B. F. SMITH, AND H. ZHANG, *PETSc/TS: A modern scalable ODE/DAE solver library*, arXiv preprint arXiv:1806.01437, (2018).
- [2] S. BALAY, S. ABHYANKAR, M. F. ADAMS, J. BROWN, P. BRUNE, K. BUSCHELMAN, L. DALCIN, A. DENER, V. ELJKHOUT, W. D. GROPP, D. KARPEYEV, D. KAUSHIK, M. G. KNEPLEY, D. A. MAY, L. C. MCINNES, R. T. MILLS, T. MUNSON, K. RUPP, P. SANAN, B. F. SMITH, S. ZAMPINI, H. ZHANG, AND H. ZHANG, *PETSc users manual*, Tech. Report ANL-95/11 - Revision 3.11, Argonne National Laboratory, 2019.
- [3] M. H. CARPENTER, T. C. FISHER, E. J. NIELSEN, AND S. H. FRANKEL, *Entropy stable spectral collocation schemes for the Navier–Stokes equations: discontinuous interfaces*, SIAM Journal on Scientific Computing, 36 (2014), pp. B835–B867.
- [4] M. H. CARPENTER, T. C. FISHER, E. J. NIELSEN, M. PARSANI, M. SVÄRD, AND N. YAMALEEV, *Entropy stable summation-by-parts formulations for computational fluid dynamics*, Handbook of Numerical Analysis, (2016), pp. 495–524.
- [5] M. H. CARPENTER, D. GOTTLIEB, AND S. ABARBANEL, *Time-stable boundary conditions for finite-difference schemes solving hyperbolic systems: Methodology and application to high-order compact schemes*, Journal of Computational Physics, 111 (1994), pp. 220–236.
- [6] M. H. CARPENTER, M. PARSANI, T. C. FISHER, AND E. J. NIELSEN, *Entropy stable staggered grid spectral collocation for the Burgers’ and compressible Navier–Stokes equations*, NASA TM-2015-218990, (2015).
- [7] M. H. CARPENTER, M. PARSANI, T. C. FISHER, AND E. J. NIELSEN, *Towards and entropy stable spectral element framework for computational fluid dynamics*, in 54th AIAA Aerospace Sciences Meeting, AIAA 2016-1058, American Institute of Aeronautics and Astronautics (AIAA), 2016.
- [8] J. CHAN, *On discretely entropy conservative and entropy stable discontinuous Galerkin methods*, Journal of Computational Physics, 362 (2018), pp. 346 – 374.
- [9] P. CHANDRASHEKAR, *Kinetic energy preserving and entropy stable finite volume schemes for compressible Euler and Navier–Stokes equations*, Communications in Computational Physics, 14 (2013), pp. 1252–1286.
- [10] T. CHEN AND C.-W. SHU, *Entropy stable high order discontinuous Galerkin methods with suitable quadrature rules for hyperbolic conservation laws*, Journal of Computational Physics, 345 (2017), pp. 427 – 461.
- [11] J. CREAN, J. E. HICKEN, D. C. DEL REY FERNÁNDEZ, D. W. ZINGG, AND M. H. CARPENTER, *Entropy-stable summation-by-parts discretization of the Euler equations on general curved elements*, Journal of Computational Physics, 356 (2018), pp. 410 –438.
- [12] C. M. DAFERMOS, *Hyperbolic conservation laws in continuum physics*, Springer-Verlag, Berlin, 2010.
- [13] L. DALCIN, D. ROJAS, S. ZAMPINI, D. C. DEL REY FERNÁNDEZ, M. H. CARPENTER, AND M. PARSANI, *Conservative and entropy stable solid wall boundary conditions for the compressible Navier–Stokes equations: Adiabatic wall and heat entropy transfer*, Journal of Computational Physics, 397 (2019).
- [14] D. C. DEL REY FERNÁNDEZ, P. D. BOOM, AND D. W. ZINGG, *A generalized framework for nodal first derivative summation-by-parts operators*, Journal of Computational Physics, 266 (2014), pp. 214–239.
- [15] D. C. DEL REY FERNÁNDEZ, M. H. CARPENTER, L. DALCIN, L. FREDRICH, A. R. WINTERS, G. J. GASSNER, S. ZAMPINI, AND M. PARSANI, *Entropy stable non-conforming discretizations with the summation-by-parts property for curvilinear coordinates*, NASA TM-2019-, (2019).
- [16] D. C. DEL REY FERNÁNDEZ, J. CREAN, M. H. CARPENTER, AND J. E. HICKEN, *Staggered entropy-stable summation-by-parts discretization of the Euler equations on general curved elements*, Journal of Computational Physics, 392 (2019), pp. 161–186.
- [17] D. C. DEL REY FERNÁNDEZ, J. E. HICKEN, AND D. W. ZINGG, *Review of summation-by-parts operators with simultaneous approximation terms for the numerical solution of partial differential equations*, Computers & Fluids, 95 (2014), pp. 171–196.
- [18] J. R. DORMAND AND P. J. PRINCE, *A family of embedded Runge–Kutta formulae*, Journal of Computational and Applied Mathematics, 6 (1980), pp. 19 – 26.
- [19] T. C. FISHER, *High-order L^2 stable multi-domain finite difference method for compressible flows*, PhD thesis, Purdue University, August 2012.
- [20] T. C. FISHER AND M. H. CARPENTER, *High-order entropy stable finite difference schemes for nonlinear conservation laws: Finite domains*, Journal of Computational Physics, 252

- (2013), pp. 518–557.
- [21] T. C. FISHER, M. H. CARPENTER, J. NORDSTRÖM, AND N. K. YAMALEEV, *Discretely conservative finite-difference formulations for nonlinear conservation laws in split form: Theory and boundary conditions*, Journal of Computational Physics, 234 (2013), pp. 353–375.
 - [22] U. S. FJORDHOLM, S. MISHRA, AND E. TADMOR, *Arbitrarily high-order accurate entropy stable essentially nonoscillatory schemes for systems of conservation laws*, Communications in Computational Physics, 50 (2012), pp. 554–573.
 - [23] L. FRIEDRICH, G. SHNÜCKE, A. R. WINTERS, D. C. DEL REY FERNÁNDEZ, G. J. GASSNER, AND M. H. CARPENTER, *Entropy stable space-time discontinuous Galerkin schemes with summation-by-parts property for hyperbolic conservation laws*, Journal of Scientific Computing, 80 (2019), pp. 175–222.
 - [24] L. FRIEDRICH, A. R. WINTERS, D. C. DEL REY FERNÁNDEZ, G. J. GASSNER, M. PARSANI, AND M. H. CARPENTER, *An entropy stable h/p non-conforming discontinuous Galerkin method with the summation-by-parts property*, Journal of Scientific Computing, (2018), pp. 1–37.
 - [25] M. GERRITSEN AND P. OLSSON, *Designing an efficient solution strategy for fluid flows 1. A stable high order finite difference scheme and sharp shock resolution for the Euler equations*, Journal of Computational Physics, 129 (1996), pp. 245–262.
 - [26] T. J. R. HUGHES, L. P. FRANCA, AND M. MALLETT, *A new finite element formulation for computational fluid dynamics, I: symmetric forms of the compressible Navier–Stokes equations and the second law of thermodynamics*, Computer Methods in Applied Mechanics and Engineering, 54 (1986), pp. 223 – 234.
 - [27] F. ISMAIL AND P. L. ROE, *Affordable, entropy-consistent Euler flux functions II: entropy production at shocks*, Journal of Computational Physics, 228 (2009), pp. 5410–5436.
 - [28] M. G. KNEPLEY AND D. A. KARPEEV, *Mesh algorithms for PDE with Sieve I: Mesh distribution*, Scientific Programming, 17 (2009), pp. 215–230.
 - [29] H.-O. KREISS AND J. OLIGER, *Comparison of accurate methods for the integration of hyperbolic equations*, Tellus, 24 (1972), pp. 199–215.
 - [30] M. L. MERRIAM, *An entropy-based approach to nonlinear stability*, NASA TM-101086, (1989).
 - [31] J. NORDSTRÖM AND M. H. CARPENTER, *Boundary and interface conditions for high-order finite-difference methods applied to the Euler and Navier–Stokes equations*, Journal of Computational Physics, 148 (1999), pp. 621–645.
 - [32] P. OLSSON AND J. OLIGER, *Energy and maximum norm estimates for nonlinear conservation laws*, Tech. Report 94–01, The Research Institute of Advanced Computer Science, 1994.
 - [33] M. PARSANI, M. H. CARPENTER, T. C. FISHER, AND E. J. NIELSEN, *Entropy stable staggered grid discontinuous spectral collocation methods of any order for the compressible Navier–Stokes equations*, SIAM Journal on Scientific Computing, 38 (2016), pp. A3129–A3162.
 - [34] M. PARSANI, M. H. CARPENTER, AND E. J. NIELSEN, *Entropy stable discontinuous interfaces coupling for the three-dimensional compressible Navier–Stokes equations*, Journal of Computational Physics, 290 (2015), pp. 132–138.
 - [35] M. PARSANI, M. H. CARPENTER, AND E. J. NIELSEN, *Entropy stable wall boundary conditions for the three-dimensional compressible Navier–Stokes equations*, Journal of Computational Physics, 292 (2015), pp. 88–113.
 - [36] H. RANOCHA, M. SAYYARI, L. DALCIN, M. PARSANI, AND D. I. KETCHESON, *Relaxation Runge–Kutta methods: Fully-discrete explicit entropy-stable schemes for the Euler and Navier–Stokes equations*, (2019). Submitted to SIAM Journal on Scientific Computing.
 - [37] D. RAY, P. CHANDRASHEKAR, U. S. FJORDHOM, AND S. MISHRA, *Entropy stable scheme on two-dimensional unstructured grids for Euler equations*, Communications in Computational Physics, 19 (2016), pp. 1111–1140.
 - [38] N. D. SANDHAM, Q. LI, AND H. C. YEE, *Entropy splitting for high-order numerical simulation of compressible turbulence*, Journal of Computational Physics, 178 (2002), pp. 307–322.
 - [39] B. SJÖRN AND H. C. YEE, *High order entropy conservative central schemes for wide ranges of compressible gas dynamics and MHD flows*, Journal of Computational Physics, 364 (2018), pp. 153–185.
 - [40] G. SÖDERLIND, *Digital filters in adaptive time-stepping*, ACM Transactions on Mathematical Software, 29 (2003), pp. 1–26.
 - [41] G. SÖDERLIND AND L. WANG, *Adaptive time-stepping and computational stability*, Journal of Computational and Applied Mathematics, 185 (2006), pp. 225–243.
 - [42] M. SVÄRD, *Weak solutions and convergent numerical schemes of modified compressible Navier–Stokes equations*, Journal of Computational Physics, 288 (2015), pp. 19–51.
 - [43] M. SVÄRD, M. H. CARPENTER, AND M. PARSANI, *Entropy stability and the no-slip wall boundary condition*, SIAM Journal on Numerical Analysis, 56 (2018), pp. 256–273.
 - [44] M. SVÄRD AND J. NORDSTRÖM, *Review of summation-by-parts schemes for initial-boundary-*

- value-problems*, Journal of Computational Physics, 268 (2014), pp. 17–38.
- [45] B. SWARTZ AND B. WENDROFF, *The relative efficiency of finite difference and finite element methods. I: Hyperbolic problems and splines*, SIAM Journal on Numerical Analysis, 11 (1974), pp. 979–993.
 - [46] E. TADMOR, *The numerical viscosity of entropy stable schemes for systems of conservation laws I*, Mathematics of Computation, 49 (1987), pp. 91–103.
 - [47] E. TADMOR, *Entropy stability theory for difference approximations of nonlinear conservation laws and related time-dependent problems*, Acta Numerica, 12 (2003), pp. 451–512.
 - [48] D. THOMAS AND C. K. LOMBARD, *Geometric conservation law and its application to flow computations on moving grids*, AIAA Journal, 17 (1979), pp. 1030–1037.
 - [49] M. VINOKUR AND H. C. YEE, *Extension of efficient low dissipation high order schemes for 3-d curvilinear moving grids*, in *Frontiers of Computational Fluid Dynamics*, D. A. Caughey and M. Hafez, eds., World Scientific Publishing Company, 2002, pp. 129–164.
 - [50] A. R. WINTERS, D. DERIGS, G. J. GASSNER, AND S. WALCH, *Uniquely defined entropy stable matrix dissipation operator for high Mach number ideal MHD and compressible Euler simulations*, Journal of Computational Physics, 332 (2017), pp. 274–289.
 - [51] A. R. WINTERS AND G. J. GASSNER, *A comparison of two entropy stable discontinuous Galerkin spectral element approximations to the shallow water equations with non-constant topography*, Journal of Computational Physics, 301 (2015), pp. 357–376.
 - [52] N. K. YAMALEEV AND M. H. CARPENTER, *A family of fourth-order entropy stable non-oscillatory spectral collocation schemes for the 1-d Navier-Stokes equations*, Journal of Computational Physics, 331 (2017), pp. 90–107.
 - [53] H. C. YEE, M. VINOKUR, AND M. J. DJOMEHRI, *Entropy splitting and numerical dissipation*, Journal of Computational Physics, 162 (2000), pp. 33–81.